Atmospheric
Chemistry
and Physics
Discussions

Open Access

Multi-model simulation of CO and HCHO in the Southern Hemisphere: biogenic emissions and model uncertainties

G. Zeng[1], J. E. Williams[2], J. A. Fisher[3], L. K. Emmons[4], N. B. Jones[3], O. Morgenstern[1], J. Robinson[1], D. Smale[1], C. Paton-Walsh[3], and D. W. T. Griffith[3]

[1]National Institute of Water and Atmospheric Research, Lauder, New Zealand
[2]Royal Netherlands Meteorological Institute, De Bilt, the Netherlands
[3]University of Wollongong, Wollongong, New South Wales, Australia
[4]National Centre for Atmospheric Research, Boulder, Colorado, USA

Correspondence to: G. Zeng (guang.zeng@niwa.co.nz)

ACPD

15, 2615–2678, 2015

Uncertainties in modelled SH CO, HCHO

G. Zeng et al.

Title Page

Abstract	Introduction
Conclusions	References
Tables	Figures

◄◄   ►►

◄   ►

Back   Close

Full Screen / Esc

Printer-friendly Version

Interactive Discussion

Full Screen / Esc

Printer-friendly Version

Interactive Discussion

Abstract

We investigate the impact of biogenic emissions on carbon monoxide (CO) and formaldehyde (HCHO) in the Southern Hemisphere (SH), with simulations using two different biogenic emission inventories for isoprene and monoterpenes. Results from four atmospheric chemistry models are compared to continous long-term ground-based CO and HCHO column measurements at SH NDACC sites, and to in situ surface CO measurements from across the SH, representing a subset of the NOAA GMD network. Simulated mean model CO using the CLM-MEGANv2.1 inventory is in good agreement with both column and surface observations, whereas simulations adopting LPJ-GUESS emissions markedly underestimate measured column and surface CO at most sites. Differences in biogenic emissions cause large differences in CO in the source regions which propagate to the remote SH. Significant inter-model differences exist in modelled column and surface CO, due mainly to differences in the models' oxidation schemes for volatile organic compounds; secondary production of CO dominates these inter-model differences. While biogenic emissions are a significant factor in modelling SH CO, inter-model differences pose an additional challenge to constrain these emissions. Corresponding comparisons of HCHO columns at two SH mid-latitude sites reveal that all models significantly underestimate the observed values by approximately a factor of 2. There is a much smaller impact on HCHO of the significantly different biogenic emissions in remote regions, compared to the source regions. Decreased biogenic emissions cause decreased CO export to remote regions, which leads to increased OH; this in turn results in increased HCHO production through methane oxidation. In agreement with earlier studies, we corroborate that significant HCHO sources are likely missing in the models in the remote SH.

1 Introduction

Carbon monoxide (CO) is ubiquitous throughout the troposphere and is an important ozone (O_3) precursor; it originates from both primary emission sources (fossil fuel and biomass combustion, biogenic and oceanic processes) and in-situ chemical production. The dominant chemical source term in the troposphere is the photo-oxidation of methane (CH_4) and non-methane volatile organic compounds (NMVOCs) (e.g., Duncan et al., 2007). Its principal sink is the reaction with the hydroxyl radical (OH), hence CO plays a key role in controlling the oxidizing capacity in the atmosphere (e.g., Levy, 1971). The oxidation of methane and NMVOCs, such as isoprene (C_5H_8), monoterpenes ($C_{10}H_{16}$), acetone (CH_3COCH_3) and higher aldehydes, leads to the formation of formaldehyde (HCHO), which, through photolysis and reaction with OH, is the major chemical source of CO (Atkinson, 2000). Once formed, CO has a relatively long lifetime of around 1–2 months, and therefore it is often used as a chemical marker for characterizing the long-range transport of air pollutants away from important source regions (e.g., Staudt et al., 2001; Heald et al., 2003; Liang et al., 2004; Fisher et al., 2010).

Due to a lack of strong regional emission sources, the Southern Hemisphere (SH) acts as a global sink for many of the polluting trace species emitted in the tropics, where polluted plumes are transported away out over the relatively clean ocean becoming subject to chemical processing. The relatively low population density, and thus low anthropogenic activity, in the SH means that direct emission sources of CO are principally limited to biomass burning (BB) and direct biogenic processes (e.g., Swinnerton et al., 1970; Watson et al., 1990; Fishman et al., 1991). Satellite and ground-based observations of CO in the SH have been used to identify the effect of BB and its footprint through long-range transport in the SH, which dominates the CO seasonal cycle there (e.g., Rinsland et al., 2005; Edwards et al., 2006; Gloudemans et al., 2006; Morgenstern et al., 2012). Biogenic VOCs are important sources of CO and HCHO in the SH, and isoprene oxidation contributes significantly to the regional CO and HCHO abundances in the SH (Pfister et al., 2008). However, large uncertainties exist in biogenic

emissions inventories, in particular for surface fluxes of isoprene and monoterpenes (Arneth et al., 2008), and the effect of such uncertainties on SH composition, such as CO and HCHO, has not been adequately assessed.

Large-scale global chemistry models are a suitable tool to investigate such sensitivities and effects on the tropospheric CO budget (e.g., Holloway et al., 2000; Duncan et al., 2007). For instance, global atmospheric models systematically overestimate observed surface CO at Cape Grim, whilst underestimate at the polluted Northern Hemisphere (NH) surface sites (e.g., Shindell et al. , 2006; Naik et al., 2013). More recently, an attempt to reconcile this underestimation in the NH CO by simply doubling either the anthropogenic CO emissions, or biogenic emissions for CO and VOCs, as well as CO BB emissions has been shown to unrealistically amplify the positive bias simulated in the SH (Stein et al., 2014), and the resulting global emission estimates employed for e.g. isoprene ($\sim 847\,\mathrm{Tg\,C\,yr^{-1}}$) are much higher than the range spanned by the various bottom-up inventories (~ 400–$600\,\mathrm{Tg\,C\,yr^{-1}}$; Arneth et al., 2008). Currently, there are large uncertainties in estimating global isoprene emissions in top-down approaches and the typical range of annual total isoprene emissions implemented in global atmospheric chemistry models is ~ 200–$600\,\mathrm{Tg\,C\,yr^{-1}}$ (e.g., Stevenson et al., 2006; Arneth et al., 2011).

Global distributions of HCHO are much more inhomogeneous than CO, due to the much shorter lifetime of HCHO (in the order of a few hours), and the concentration of HCHO drops off sharply away from the source regions. HCHO is commonly used to constrain isoprene emissions in high-emission regions, because it is a high-yield product of isoprene oxidation (e.g., Palmer et al., 2003; Shim et al., 2005; Barkley et al., 2008). A recent study by Marais et al. (2014) compares isoprene emissions inferred using retrieved HCHO columns from the Ozone Monitoring Instrument (OMI) to the MEGAN (Guenther et al., 2012) values and finds that OMI-derived emissions are lower than the values from MEGAN over the African continent. However, ground-based HCHO measurements over the SH are sparse, and the extremely low concentrations over the remote oceans complicate comparisons of model results with observations.

For example, HCHO columns observed at Lauder (Jones et al., 2009) and at Re-union Island (Vigouroux et al., 2009) cannot be satisfactorily reproduced by the models (where a box model was used to simulate HCHO concentrations at Lauder), with modelled HCHO being generally substantially low-biased.

In this study, we build on these previous investigations by conducting a number of simulations using an ensemble of transport models (CTMs) and chemistry–climate models (CCMs) as part of the Southern Hemisphere Model Intercomparison Project (SHMIP). Given the relatively low anthropogenic emissions in the SH and the dominance of biogenic emissions of VOCs (mainly isoprene), we determine the influence that different emission inventories of isoprene and monoterpenes have regarding their effects on modelled CO and HCHO columns in the SH. Satellite observations of SH CO usually are in good agreement with ground-based observations, however the data quality of the satellite data deteriorates towards the poles (Morgenstern et al., 2012). They find that CO columns exhibit a large-scale mode of variability in the remote SH that does not exist in the NH. For our purposes, we make use of high-precision ground-based Fourier Transform Infrared Spectroscopy (FTIR) measurements of CO columns from four SH sites that have not previously been fully exploited for model evaluations, namely Darwin (12.43° S, 130.89° E) and Wollongong (34.41° S, 150.88° E) in Australia, Lauder (45.04° S, 169.69° E) in New Zealand, and Arrival Heights (77.82° S, 166.65° E) in Antarctica. We also compare the modelled HCHO columns to those observed by the FTIR instruments at Wollongong and Lauder. In a companion paper, Fisher et al. (2014) have evaluated the vertical gradients of CO from the SHMIP models in the vicinity of Cape Grim, Australia, which is representative of SH mid-latitude background air, using multi-year aircraft measurements available from the Cape Grim Overflight Programme (Langenfelds et al., 1996). The influence of both chemistry and transport on the modelled vertical gradients of CO are addressed. Although there are biases of various magnitudes across the different models, the seasonal variability and extent of the gradients in tropospheric CO are shown to be captured reasonably well, especially during the tropical BB season.

In this paper we address the sensitivity of CO and HCHO distributions in the SH to biogenic emissions of isoprene and monoterpenes as provided by the LPJ-GUESS inventory (Arneth et al., 2007a, b; Schurgers et al., 2009) and the MEGANv2.1 model (Guenther et al., 2012) across the models included in SHMIP. In Sect. 2 we provide model descriptions, the common emission inventories used to drive the models, and the observations used in the study. In Sect. 3 we compare results for the period 2004–2008 and show comparisons between modelled CO and HCHO columns and the FTIR measurements at the four SH sites mentioned above, as well as comparisons between modelled and observed surface CO. In Sect. 4 we analyse differences in the models' abilities to reproduce SH CO and HCHO columns, and the underlying differences in the models' chemistry and transport. In Sect. 5 we assess the sensitivity of modelled CO and HCHO to changes in biogenic emissions and the effect of such changes on the oxidizing capacity in the clean SH. Finally, in Sect. 6 we present our conclusions.

2 Model simulations and observations

The SHMIP intercomparison uses four global models, including two CTMs (TM5, GEOS-Chem) and two CCMs (CAM-chem, NIWA-UKCA). In this section we provide the description of the simulations performed, the common emissions inventories employed, a brief description of each model, the meteorological drivers, and the observations used for evaluating the performance of the models.

2.1 Simulations

We perform simulations covering the period of 2004 to 2008 using a one-year spin-up for 2003. The two CTMs are driven by the meteorological analysis for the same period from their respective sources, whereas NIWA-UKCA uses observed sea surface temperature and sea ice data sets. CAM-chem runs in the specified-dynamics mode, using meteorological fields from reanalysis data. Two simulations are performed in all

Full Screen / Esc

Printer-friendly Version

Interactive Discussion

models with identical emission inventories for the anthropogenic and BB components, but different inventories are adopted for biogenic isoprene and monoterpene emissions. We also include passive CO tracers in the simulation defined as having the same global primary, surface emission sources as CO, but with one having a fixed lifetime of 25 days and a second having the lifetime determined by OH distribution in each respective model. These tracers allow the differentiation of the inter-model variability with respect to transport of CO to the SH from the main source regions.

Although we have been careful to harmonize the emissions used across models, differences in the chemical mechanisms which are employed result in the aggregated emissions of the NMVOCs being somewhat different across the ensemble. For anthropogenic emissions, we adopt the yearly specific MACCity global emission estimates (Lamarque et al., 2010; Granier et al., 2011) nested with the Regional Emission Inventory in Asia (REASv2.1) for the East Asia region (Kurokawa et al., 2013). Interannually varying monthly mean BB emissions are taken from the Global Fire Emissions Database version 3 (GFEDv3) (van der Werf et al., 2010). For lightning-NO_x emissions, each model adopts individual parameterizations, and soil-NO_x is taken from the MACCity inventory. Biogenic emissions for isoprene, monoterpenes, CO, methanol, and acetone are based on MEGANv2.1 (Guenther et al., 2012) and are calculated offline using the Community Land Model (CLM4.0; Lawrence et al., 2011) (we refer this dataset as CLM-MEGANv2.1 hereafter). We then replace the MEGANv2.1 emissions for isoprene and monoterpenes with the GUESS-ES emissions (Arneth et al., 2007a; Schurgers et al., 2009) (http://eccad.sedoo.fr) in our second set of simulations for comparison (hereafter referred to as LPJ-GUESS emissions). None of the models currently include any higher terpenes. Other natural emissions such as CO emitted from the ocean are specified independently in each model. The annual total emission fluxes for key species are listed in Table 1 for the simulation period of 2004–2008. The yearly-varying annual total emissions of isoprene from CLM-MEGANv2.1 are markedly larger than the LPJ-GUESS emissions ($\sim$ 5–10 % relative to CLM-MEGANv2.1), and the corresponding differences are much larger for the SH between these two inven-

Uncertainties in modelled SH CO, HCHO

G. Zeng et al.

|◄ | ►|

◄ | ►

Back | Close

Full Screen / Esc

Printer-friendly Version

Interactive Discussion

tories, i.e. ~ 10–20 % over the same period. For monoterpenes the CLM-MEGANv2.1 emissions are substantially larger than the LPJ-GUESS emissions globally. Figure 1 shows the SH and regional monthly total isoprene emission fluxes from LPJ-GUESS and CLM-MEGANv2.1 for Australia and part of Indonesia (0–44° S, 94–156° E), Southern Africa (0–37° S, 9–44° E) and South America (0–57° S, 34–84° W), the regions with high isoprene emissions. The largest monthly emissions occur in austral summer in both datasets when the differences between these two datasets are also largest. Overall CLM-MEGANv2.1 isoprene emissions (especially the summer maxima) are substantially higher than LPJ-GUESS emissions with the exception of S. Africa, where LPJ-GUESS emissions are larger. Figure 2 shows the differences in the spatial distribution of the fluxes for both isoprene and monoterpenes for January 2005. There are elevated emissions in Amazonia, southern Africa, and Australia in CLM-MEGANv2.1 that do not occur in the LPJ-GUESS emissions.

2.2 Models

2.2.1 NIWA-UKCA

NIWA-UKCA stands for the version of the UK Chemistry and Aerosols Model (UKCA) that is used and further developed at the National Institute of Water and Atmospheric Research (NIWA). The background climate model is similar to HADGEM3-A (Hewitt et al., 2011) with a horizontal resolution of $3.75° \times 2.5°$ and 60 vertical levels extending from the surface to 84 km. The physical processes in NIWA-UKCA, including interactive dry and wet deposition of the trace gases and the FAST-JX photolysis scheme, have been described in detail by Morgenstern et al. (2013) and O'Connor et al. (2014). Unlike the version described by O'Connor et al. (2014), here we now apply dry deposition following Wesely (1989) only to the bottom model layer rather than throughout the boundary layer. The model setup used here comprises a coupled stratosphere–troposphere chemistry scheme. The stratospheric reactions are the same as in Morgenstern et al. (2009) and include explicit chlorine and bromine chemistry. We have up-

dated the NIWA-UKCA chemical mechanism from that described in Morgenstern et al. (2013) to account for emissions and degradations of ethene (C_2H_4), propene (C_3H_6), methanol (CH_3OH), isoprene, a representative monoterpene, and a lumped species that accounts for missing NMVOCs in the model similar to the approach taken in the IMAGES model (Müller and Brasseur, 1995), with primary emission sources. In addition to the above, the NIWA-UKCA chemical scheme includes nitrogen oxides (NO_x), CO, ethane (C_2H_6), propane (C_3H_8), HCHO, acetone (CH_3COCH_3), and acetaldehyde (CH_3CHO) as primarily emitted species (O'Connor et al., 2014). The isoprene oxidation scheme is the mechanism described by Pöschl et al. (2000), as previously used by Zeng et al. (2008), but with rate coefficients of reactions between OH and isoprene nitrates and between NO and isoprene peroxy radicals updated following Paulot et al. (2009a, b). We adopt the very simple monoterpene oxidation scheme described by Brasseur et al. (1998). Methane mixing ratios are prescribed at the surface with a slight north-to-south gradient of 1813 ppbv north of the Equator and 1707 ppbv south of the Equator. Surface emissions are as specified in Sect. 2.1. Lightning NO emissions are based on the parameterization of Price and Rind (1992, 1994), as a function of convection. The model uses prescribed sea surface conditions following the Atmospheric Model Intercomparison Project (AMIP) II (http://www-pcmdi.llnl.gov). The chemistry is run in a semi-offline mode, i.e. chemistry feedbacks to meteorology and hydrology are deactivated. Table 2 summarizes key model properties for all models.

2.2.2 TM5

TM5 is a global 3-D CTM driven by meteorological fields from the ECMWF ERA-interim re-analysis (Dee et al., 2011) using an update frequency of three hours. Interpolated fields are used for the interstitial time periods. The version used here is identical to that described by Williams et al. (2014) and uses the modified CB05 chemical mechanism (Williams et al., 2013) for describing the chemistry which occurs in the troposphere, along with online photolysis rates. Details relating to the convection, advection and deposition processes employed are given by Huijnen et al. (2010). TM5 includes a full

description of HO_x and NO_x reactions, as well as explicitly treating all C1 to C3 organic species in addition to ammonia (NH_3), sulphur dioxide (SO_2) and dimethyl sulphide (DMS). For this study a horizontal resolution of $3° \times 2°$ is chosen adopting 34 vertical layers from the surface up to 0.5 hPa. The isoprene and monoterpene oxidation schemes are based on the mechanisms developed by Yarwood et al. (2005), with modifications following recommendations by Archibald et al. (2010). Methane emissions are included and the simulated surface concentrations are then nudged towards a latitudinally and monthly varying climatology based on surface observations; a detailed description of the approach is given by Williams et al. (2013).

2.2.3 GEOS-Chem

The GEOS-Chem global 3-D CTM (www.geos-chem.org) is driven by meteorology from the NASA Global Monitoring and Assimilation Office (GMAO) Goddard Earth Observing System (GEOS-5) assimilated product (Bey et al., 2001). The native GEOS-5 product with $0.667° \times 0.5°$ horizontal resolution and 72 vertical levels (surface to 0.01 hPa) is regridded for computational efficiency to $2.5° \times 2° \times 47$ levels (with all vertical lumping in the stratosphere). Here we use the v9-01-03 coupled O_3–NO_x–HO_x–VOC–aerosol simulation with the Caltech isoprene mechanism (Paulot et al., 2009a, b), which includes 57 transported species (both gas-phase and aerosol) and an additional 49 species that interact chemically but are not transported. As monoterpenes are not included as an explicit chemical species, their emissions are used to produce CO (assumed 20 % molar yield; Duncan et al., 2007) and acetone (assume a 12 % molar yield; Jacob et al., 2002). CH_4 mixing ratios are prescribed annually and latitudinally based on NOAA GMD surface observations. Interactive chemistry is computed in the troposphere only, with stratosphere production and loss rates for most species taken from the NASA Global Modeling Initiative (GMI) Combo CTM Aura4 model (Murray et al., 2013). Stratospheric ozone is simulated using the Linoz linearized ozone scheme (McLinden et al., 2000). Lightning NO emissions are based on the cloud top height parameterization of Price and Rind (1992) with regional correction to match lightning distributions from

satellite, as described by Murray et al. (2012). Other processes in GEOS-Chem v9-01-03 including mixing and deposition are described in detail by Mao et al. (2010, 2013a). The version used here was modified from the standard v9-01-03 to include irreversible HO_2 uptake by aerosols with a gamma value of 0.2 (Mao et al., 2013b), and to include methanol as an interactive tracer based on the offline simulation of Millet et al. (2008). In the standard GEOS-Chem simulation, biogenic emissions are computed on-line using a coupled version of the MEGAN model. Here, to ensure consistency with the other SHMIP models, we used the pre-computed biogenic emissions described above (Sect. 2.1) and applied an imposed diurnal variability tied to solar zenith angle.

2.2.4   CAM-chem

The Community Atmosphere Model with Chemistry (CAM-chem) is a component of the NCAR Community Earth System Model (CESM). The version used for this study is the same as that used for the Chemistry–Climate Model Initiative (CCMI) (Eyring et al., 2013), and very similar to that described in Lamarque et al. (2012). For SHMIP, CAM-chem was run in the specified dynamics mode, using meteorological fields from the Modern-Era Retrospective Analysis For Research And Applications (MERRA) re-analysis product (http://gmao.gsfc.nasa.gov/merra/), regridded to the model horizontal resolution of 1.9° × 2.5°, using the lowest 56 levels. In this study, the internally derived meteorological fields (temperature, winds, surface heat and water fluxes) are nudged at every time step (30 min) by 1 % towards the reanalysis fields (i.e., a 50 h Newtonian relaxation time). The chemical mechanism, based on MOZART-4 (Emmons et al., 2010) includes both tropospheric and stratospheric chemistry, with 150 compounds and 400 photolysis and kinetic reactions, and a tropospheric bulk aerosol model (Lamarque et al., 2012). Heterogeneous reactions on aerosols are included as described in Emmons et al. (2010), including the uptake of HO_2 with a reaction probability of 0.2 producing H_2O_2. While the option of running with online MEGANv2.1 biogenic emissions is available in CAM-chem, this was not used and all surface emissions were based on those specified for this intercomparison, with diurnal variation imposed for isoprene

and monoterpenes. Methane surface mixing ratios are specified for monthly zonal averages, as used for CCMI, based on RCP6.0 (Meinshausen et al., 2011). Lightning NO emissions are determined according to the cloud height parameterization of Price and Rind (1992) and Price et al. (1997). The vertical distribution follows DeCaria et al. (2006) and the strengths of intra-cloud and cloud-ground strikes are assumed equal, as recommended by Ridley et al. (2005).

2.3 Observations of CO and HCHO in the SH

Long-term measurements of trace gases up to the upper troposphere in the remote SH are sparse. Continuous multi-year tropospheric columns of CO are observed at four SH sites: Darwin, Wollongong, Lauder, and Arrival Heights, with high spectral resolution FTIR spectrometers. In addition, HCHO columns have been retrieved at Wollongong and Lauder. The data records and retrieval methods have largely been presented before (Rinsland et al., 1998, 2002; Jones et al., 2001, 2009; Paton-Walsh et al., 2010; de Laat et al., 2006; Zeng et al., 2012; Morgenstern et al., 2012) and therefore we only give a brief description here.

At Wollongong, Lauder, and Arrival Heights, mid-infrared (MIR) spectra from the FTIR measurements are used to retrieve CO columns, and these stations are part of the Network for the Detection of Atmospheric Composition Change (NDACC; http://www.ndacc.org). The retrieval of trace gas information from these recorded spectra was performed based on the SFIT2 profile retrieval algorithm using the 4.7 µm band, and is similar to that described by Rinsland et al. (1998, 2002). At Arrival Heights, there are no measurements during the polar nights which last 4–5 months per year. CO total columns have been observed at Darwin since 2005 with solar remote sensing using FTIR measurements in the near infrared (NIR), as part of the Total Column Carbon Observing Network (TCCON) (Deutscher et al., 2010; Wunch et al., 2011). The spectra used for CO retrieval are analysed with the GFIT spectral fitting algorithm (Washenfelder et al., 2006) for total column CO. Details of the retrieval method and data are described in Paton-Walsh et al. (2010). Daily averaged time series of CO

Full Screen / Esc

Printer-friendly Version

Interactive Discussion

columns from 2004 to 2008 are used for comparison with the models. Due to the very small "smoothing" error for CO retrievals, which indicates the difference between realistic and retrieved CO columns, averaging kernels are not applied when comparing with the modelled CO data (de Laat et al., 2006; Zeng et al., 2012). Comparisons are made against daily output from each model to ensure that variability in the transport component is well captured.

Total columns of HCHO were retrieved at Wollongong and Lauder from the mid-infrared spectra using the SFIT2 inversion algorithm (Jones et al., 2009). HCHO is a very weak absorber in the mid-infrared spectral region. Due to its large "smoothing" errors, the averaging kernels and a priori applied in the retrieval were also applied to the modelled data for a like-with-like comparison between the modelled and retrieved HCHO columns following the method described by Zeng et al. (2012) and references therein.

In order to provide comparisons on a larger spatial scale, we also perform multi-year comparisons for surface CO against flask measurements available from the NOAA Global Monitoring Division network (Novelli et al., 1998). The selected sites are all situated in the SH and cover an extensive latitudinal range. They are typically located away from regions which exhibit strong local emissions of CO; the data therefore reflect the cumulative effects of differences in both transport and chemical processing across the participating models. The sites shown are Mahe Island (4.7° S, 55.5° E), Ascension Island (8.0° S, 14.4° W), Cape Grim (40.7° S, 144.7° E), Baring Head (41.4° S, 174.9° E), Crozet Island (46.4° S, 51.9° E), Tierra del Fuego (54.9° S, 68.3° W), Syowa Station (69.0° S, 39.6° E) and South Pole (90° S, 24.8° W).

3 Comparison between models and observations

3.1 CO columns

Figure 3 shows the direct comparison between modelled and FTIR CO columns for the CLM-MEGANv2.1 simulation. Due to the significant contribution of CO from the meso-
sphere during polar spring (Velazco et al., 2007) and lack of mesospheric chemistry across all models, FTIR CO partial columns (0–12 km) are used for comparison at Arrival Heights, Lauder, and Wollongong instead of total columns. Partial columns of CO at Darwin are not available so we use total columns for comparison. At all locations, CO seasonal cycles are well reproduced by all four models. Models accurately reproduce
the total columns of CO at Darwin with very small inter-model differences. The Darwin measurement site is the closest to the tropical source regions; this indicates that the emissions in this area are well represented in the models. Inter-model differences are notably larger at other sites which are located further from the source regions, with consistent overestimation by TM5 and underestimation by CAM-chem at both Arrival
Heights and Lauder. Such differences are possibly associated with both differences in the oxidative capacities in these two models and differences in transport (discussed in Sect. 4). All models underestimate CO columns at Wollongong, especially during the peak BB season; this may be due to its proximity to large forested areas and/or the cities of Sydney and Wollongong whose direct emissions may be underestimated in
the MACCity inventory. Note that due to the coastal location of Wollongong, model grid boxes may not be representative of the measurement site.

We performed a second set of simulations using LPJ-GUESS isoprene and monoter-pene emissions; the deviation of model ensemble-mean CO columns from the observed FTIR columns are shown at the four measurement sites (Fig. 4) in compari-
son with the simulation using CLM-MEGANv2.1 biogenic emissions. The differences between these two simulations are also shown (i.e. CLM-MEGANv2.1 minus LPJ-GUESS). It appears that a larger negative bias exists when adopting the LPJ-GUESS emissions for all of the column measurement stations (i.e. CLM-MEGANv2.1 results

in better agreement with the FTIR observations). The deviations of both simulations from the observed CO columns exhibit large seasonal variations but seasonal and inter-annual variations are consistent between these two simulations.

Figure 5 shows differences between the modelled and observed FTIR CO columns at the four measurement sites from the multi-annual ensemble mean data for both CLM-MEGANv2.1 and LPJ-GUESS simulations. As in Fig. 4, the seasonal variations of the biases from these two sets of simulations follow a very similar pattern, implying that the effect of different biogenic emissions is reflected in the differences in the background CO columns in the SH. The biases shown in the ensemble model means from both simulations are largest during the SH tropical BB season of September, October and November (SON), although at Darwin the negative biases are also high in July and increase from October to December. For Wollongong, Lauder, and Arrival Heights the largest negative biases are in October, November, and December, respectively; this suggests an underestimation of SH BB sources in GFEDv3 and the subsequent effect on CO columns at SH remote locations through long-range transport. At Darwin, CO columns are more likely influenced by local or nearby BB sources which may have a different seasonality. The averaged biases of the model ensemble means for each site are shown in Table 3; the lowest biases are at Arrival Heights for both simulations which are followed by those for Darwin, Lauder, and Wollongong.

The individual model biases are also shown in Fig. 5. For both simulations, inter-model variability is notably larger during months that lie outside the seasons when most intensive BB occurs, i.e. typically in austral summer and autumn (covering December and January to May). Such seasonal dependence of inter-model variability is consistent with that described in Fisher et al. (2014) when comparing modelled vertical CO gradients in the Cape Grim region using the same simulations. Inter-model variability is generally larger in CLM-MEGANv2.1 than in LPJ-GUESS for all seasons and locations.

Full Screen / Esc

Printer-friendly Version

Interactive Discussion

3.2 Surface CO

To assess the models' ability to capture both the seasonality and inter-annual variability of CO at the surface over the simulation period, we show in Fig. 6 comparisons between the CLM-MEGANv2.1 simulations and monthly mean CO values observed at the eight surface sites listed in Sect. 2.3. Consistent with the FTIR column comparisons, all models capture the seasonal cycles of observed surface CO at each location. In line with Fig. 3 in Fisher et al. (2014), TM5 typically exhibits a high bias and CAM-Chem exhibits a low bias of the order of 5–10 ppbv. Large variations exist in seasonal cycles at both Mahe Island and Ascension Island, but the timing of the peaks are different. At Mahe Island, surface CO peaks in January and February due to the influence of anthropogenic emissions from India (Wai et al., 2014), whereas at Ascension Island, the seasonal cycle is principally driven by CO which originates from BB in Southern Africa during June-July-August (e.g., Williams et al., 2012; Wai et al., 2014). The inter-annual variability and timing in peak mixing ratios is not captured well at Ascension Island, especially for GEOS-Chem and TM5; this is possibly related to too strong westerly transport out of southern Africa and too weak an oxidative capacity, especially in TM5. For the more southerly, oceanic sites, the seasonal cycles and amplitudes are remarkably similar, indicating that the variability in background CO is rather low at the surface in the SH remote locations. The large anomalies in modelled surface CO at Cape Grim between late 2006 and the first few months of 2007 are most likely due to the 2006–2007 intense Australian bush fires. However, such enhancements in surface CO do not occur in the observed data because measurements at Cape Grim are only sampled during clean air "baseline" conditions that are not influenced by polluted air from mainland Australia, whereas modelled values are monthly means. Note that the models' grid boxes usually cover larger areas that account for biomass burning emissions. In general, NIWA-UKCA and GEOS-Chem display a better agreement with the observations in the remote SH, indicating that their oxidative capacities are more re-

Title Page

Abstract | Introduction

Conclusions | References

Tables | Figures

|◄ | ►|

◄ | ►

Back | Close

Full Screen / Esc

Printer-friendly Version

Interactive Discussion

alistic. The consistent high and low biases in TM5 and CAM-Chem, respectively, are related to the oxidizing capacity in these models; this is discussed in Sect. 4.

We quantify the differences between the multi-annual ensemble means for surface CO and the corresponding values derived from the observations for both the CLM-MEGANv2.1 and the LPJ-GUESS simulations (Fig. 7). As for the FTIR comparisons, the observed distributions of surface CO in the SH are better reproduced by CLM-MEGANv2.1 for most of the chosen sites. A comparison of sites shows that the seasonal biases are more variable for the tropical sites which are affected by the inter-annual variability in tropical BB. The positive bias at Cape Grim is caused by the models episodically simulating polluted air from the Australian continent but the measurements only sampling clean air as stated above, and the large deviation shown for December, January to March are dominated by the spikes caused by the 2006/2007 intense Australian bush fires shown in Fig. 6. For the higher-latitude sites, the bias in the ensemble for CLM-MEGANv2.1 is only of the order of a few percent, providing confidence that the ensemble mean can be used to assess the accuracy of the different biogenic emission inventories. Note that the difference between the multi-model ensemble means increases towards JJA at the sites outside the tropics; this shows that although background CO across the SH mid- to high latitudes has similar sensitivity to changes in tropical biogenic emissions, the sensitivity is somewhat larger in austral winter and spring; this is likely due to longer CO lifetimes in these seasons.

3.3 HCHO columns

Here we examine the models' ability to reproduce observed HCHO columns at the SH mid-latitude sites Lauder and Wollongong. Figure 8 shows comparisons between modelled daily mean HCHO columns convolved with FTIR a priori data and averaging kernels, and observed daily mean HCHO columns from the FTIR measurements. The seasonal cycles are generally well reproduced across the entire model ensemble, with the seaonal maxima in austral summer and the minima in winter, but all models significantly underestimate observed columns in all seasons. Inter-model differences in

modelled HCHO columns are larger at Lauder than at Wollongong; the highest HCHO columns are produced in GEOS-Chem, whereas the lowest are from TM5. The significant and persistent low bias across all models cannot be reconciled by considering the diurnal cycle in HCHO; for testing purposes, we also calculated HCHO columns by replacing daily mean HCHO data shown in Fig. 8 with the daily maximum of the 3 hourly data from one of the ensemble members (CAM-chem). This resulted in small changes only ($\sim$ 10–15 % increases in certain summer months). Therefore we are confident that using daily mean modelled HCHO columns for comparing to columns from FTIR observations that occur during the daylight is satisfactory. Figure 9 shows the multi-annual mean FTIR HCHO columns and model ensemble means averaged for the same years with both CLM-MEGANv2.1 and LPJ-GUESS emissions for isoprene and monoterpenes. Overall, the models underestimate the observed HCHO columns by approximately 50 %. Differences in biogenic emissions do not appreciably affect this.

In the case of Wollongong, proximity to Sydney and the influence of episodic BB events in the vicinity (Williamson et al., 2013) could introduce local direct and indirect sources of HCHO and chemical precursors which are unaccounted for and might have contributed to the low bias simulated in the models, particularly for the seasonal peaks. However, at Lauder there are no known significant local sources of HCHO. We therefore assume that the underestimation of observed FTIR HCHO columns by the models is very likely related to missing emissions of precursors. One possible candidate could be methanol oxidation. Methanol is thought to be a significant chemical source of HCHO in remote regions, although the sources and sinks of methanol are poorly understood. Recent global estimates derived from satellite observations suggest a slightly higher global surface flux of 122 Tg yr^{-1} (Wells et al., 2014), rather than the 100 Tg yr^{-1} used here. Previous investigations involving the simulation of regional HCHO measurements taken at Cape Grim (Ayers et al., 1997), using a chemical box model assuming a 100 % yield of CH_3OOH from $CH_3O_2 + HO_2$, have also not been able to capture the magnitude of the observed mixing ratios of HCHO. Ayers et al. (1997) also experimented with an alternative oxidation pathway that involved the direct production

of HCHO (40 %) from $CH_3O_2 + HO_2$, which resulted in a much improved comparison. The model ensemble includes chemical mechanisms which presently assume either a 10 % direct yield of HCHO (NIWA-UKCA) or no direct yield in the other 3 models. The recent IUPAC recommendations (Atkinson et al., 2006) assume a temperature-dependent branching ratio for the direct HCHO production channel (i.e. 0.09 to 0.29 for temperatures ranging from 298 to 218 K). Adopting this recommendation, an additional test was performed in TM5, showing some modest increases in HCHO in the extra-tropics of up to ~ 10 %. However this is not sufficient to explain the large bias shown here. Another hypothesis mentioned by Ayers et al. (1997) is the possibility of a small marine biological source of isoprene (e.g., Bonsang et al., 1992), although global emission fluxes are estimated to be low (Arnold et al., 2009). Recently, Lawson et al. (2014) found relatively abundant HCHO precursors (dicarbonyls) in two regions of the southwest Pacific, corroborating the hypothesis that marine biological activity might be responsible for the measured HCHO abundance. However, spatial sampling and understanding of the underlying biological processes remain poor.

The HCHO column dataset we use here is an extension of the 1992–2005 dataset described by Jones et al. (2009), retrieved using the same algorithm. They performed a box model simulation and pointed out that methane oxidation alone cannot explain the significant underestimation of measured FTIR HCHO columns at Lauder, and suggested that additional local sources, possibly isoprene, are needed to explain the observed HCHO columns at Lauder. Moreover, the comparison made between modelled HCHO columns from the IMAGESv2 model and the observed FTIR HCHO columns at Reunion Island also shows an underestimation of FTIR HCHO (Vigouroux et al., 2009) albeit with a smaller magnitude than that shown here. The time series shown by Vigouroux et al. (2009) are for August to November 2004 and for May to November 2007, and the differences between modelled and observed HCHO columns are around 30 and 25 % respectively. They also include methane oxidation by tropospheric chlorine, but the impact of this process on HCHO columns is only about 1–2 % and therefore cannot explain the underestimation. However, they also experiment using

a different OH climatology; this reduced OH abundance results in better agreement between observed and modelled HCHO columns. This finding nevertheless suggests that the underestimation of HCHO columns is pertinent throughout the SH. Observations of HCHO in the remote SH regions are extremely sparse; it impossible to fully constrain modelled HCHO. Note that in both studies, FTIR HCHO columns compare well with satellite measurements (Jones et al., 2009) and with both satellite and MAX-DOAS measurements, respectively (Vigouroux et al., 2009). This suggests that the FTIR HCHO retrieval at all sites is robust, and that the likely cause for model-observation differnces is missing sources of HCHO and/or its precursors in the models.

4   Model differences in chemistry and transport

Although the four models are constrained by the same emissions, there are significant differences in the models' ability to reproduce observed CO columns and surface CO in the remote SH, as shown above. Here we explore the underlying factors driving these differences. To diagnose the extent of differences in transport between the models, we examine the two passive CO tracers defined in Sect. 2: one with a fixed lifetime of 25 days (referred to as CO_{25}) and the second with first-order loss via model calculated OH (referred to as CO_{OH}). Both tracers are subjected to the same surface emissions as the full simulations, but not subjected to any secondary production of CO from methane and NMVOC oxidation. Dry deposition of CO is not included for either of the additional CO tracers as it is considered a minor loss channel for the SH.

The global tropospheric CO columns from all models for January and September are shown in Fig. 10. Here, we define the tropospheric columns as the columns below the chemical tropopause marked by the 150 ppbv O_3 isopleth in each model (monthly mean O_3 used here is averaged over 2004–2008). Although here we focus on the SH, we note that the inter-model differences apparent in the SH are consistent with those occurring in the NH, namely, the lowest CO columns occur in CAM-chem, followed by NIWA-UKCA, with higher CO columns from GEOS-Chem and TM5 for both

hemispheres indicating systematic differences between the models. Comparing the seasonal variations, CO columns are generally higher in September than in January in the SH, primarily due to the timing of the most intensive tropical BB events in austral spring. Of the four models, CAM-chem simulates the lowest CO columns in both the source regions and in the remote mid- to high latitudes. Examining the distributions of the tropospheric columns of CO_{25} shown in Fig. 11, CO_{25} exhibit similar distributions among the models for both seasons in source regions as those shown in Fig. 10. The differences become more obvious in the extratropics, with NIWA-UKCA showing slightly weaker transport towards the poles, whereas GEOS-Chem shows somewhat stronger export of CO_{25} out of the source regions and towards the poles. Overall, despite some differences, the magnitude and distribution of CO_{25} are very similar among the models. However, such differences and similarities in transport among the models are not reflected in the differences in CO columns shown in Fig. 10 in which TM5 simulates the highest CO columns and CAM-chem the lowest in both the source and remote regions.

Next, we quantify the roles of transport and chemistry in determining the inter-model variability in the CO columns in the SH, by examining three zonal bands defined as 0–30° S, 30–60° S, and 60–90° S. These latitude bands capture the main tropical source region and mid- and high latitudes, respectively. The monthly mean tropospheric columns of CO, as well as ratios of CO_{25}/CO and CO_{OH}/CO columns, averaged across each of these zones for each model are shown in Fig. 12. $CO_{sec} = CO - CO_{OH}$ is an estimate of the fraction of CO that is produced by oxidation of CH_4 and NMVOCs; the ratio of CO_{sec} to CO is also shown in Fig. 12. These ratios define the contributions of CO_{25}, CO_{OH}, and CO_{sec} to the total CO columns in each model. Fig. 12 shows that CO columns decrease towars the high latitudes and the seasonal maxima are during the September/October BB season in all zones. Although CO_{25} is an idealized tracer designed to diagnose differences in the long-range transport simulated in each model, CO_{OH} should be a more realistic measure of how much primary emissions of CO contribute to the CO columns, because CO_{OH} reflects the locally varying lifetime of CO due

to the spatial variability of OH. The ratio of CO_{25} to CO drops sharply from the tropics to the pole for all models (from ~ 20 to $\sim 5\%$ in the annual average), as would be expected from the hemispheric distribution of emissions and the timescales for meridional transport. By contrast CO_{OH}/CO reduces only from ~ 30 to $\sim 25\%$ in the yearly average. This refelcts that the lifetime of CO is considerably longer outside of the source region due to lower background O_3 levels (and therefore lower OH levels) in the more pristine environment away from strong NO_x sources. CO_{sec}/CO shows a moderate increase from 70 to 75 % from the tropical zone to the high latitudes. Overall, primarily-emitted CO makes up ~ 25–45% of total tropospheric CO in the source region and ~ 20–40% in the polar region, depending on season, while the secondary CO makes up the remainder of the tropospheric columns, i.e. ~ 55–75% in the source region and ~ 60–80% in the polar region. Regarding seasonal variability, CO_{25} and CO_{OH} have proportionally larger contributions in austral spring when BB dominates the CO emissions, whereas CO_{sec} shows larger contributions in austral summer/autumn. Of all the models, NIWA-UKCA shows the smallest contribution from primary CO to the columns and the largest contribution from the secondary CO, relative to the other three models.

Inter-model differences in CO columns and the additional CO tracers are expressed as the ratio of individual model columns vs. the multi-model mean columns for each zone, shown in Fig. 13. For CO columns, the inter-model differences are smallest in the tropical zone and gradually increase towards the pole, with the highest CO columns from TM5 and the lowest from CAM-chem, in correspondence with the FTIR comparisons and the surface comparisons shown earlier. Examining the inter-model differences in CO_{25}, the model spread increases substantially towards the polar zone, and is characterized by the strongest transport out of the source region from GEOS-Chem and the weakest from NIWA-UKCA (also shown in Fig. 11). Note that this behaviour is not reflected in the model spread of CO columns (i.e. the highest CO occurs in TM5 and the lowest in CAM-chem). By contrast, the patterns of model spread in CO_{sec} and to a lesser degree in CO_{OH} are consistent with that seen in the CO columns, indicating that the inter-model differences in modelled CO columns are strongly influenced

by the differences in CO_{sec}, which is dependent on the oxidizing capacity in the model that also drives the loss of primary-emitted CO by OH. Considering also the absolute contributions of both primary CO sources and secondary CO production to the SH CO columns (these being ~ 35 and $\sim 65\%$, respectively), we can derive that inter-model differences in CO columns are attributed about 1/3 to primary and 2/3 to the secondary CO production in the SH. Note that here we only take into account the accumulated effects of primary and secondary contributions to CO; we do not differentiate or individually identify the separate influences e.g. of transport and chemistry. For example, the large CO columns in TM5 can be the result of combined effects of slower chemical loss of CO due to lower OH levels in the model and a faster secondary CO production in the source region, as reflected in higher ratios of CO_{sec} to CO shown in Fig. 13. In contrast, GEOS-Chem CO has faster loss by OH than TM5 (but slower than the others), but this is outweighed by a stronger transport resulting in higher CO compared to those in NIWA-UKCA and in CAM-chem. For CAM-chem, moderately slow transport of CO out of the source region combined with slower secondary CO production result in the lowest CO columns. It is possible that conversion from higher VOCs, e.g. isoprene, to CO is faster in TM5 due to the lumping of compounds in its chemical mechanism.

Apart from methane oxidation, isoprene oxidation dominates the secondary CO production in the SH (Pfister et al., 2008). Therefore it is critical to understand the differences in isoprene oxidation mechanisms between the models. However, this is beyond the scope in this study. Archibald et al. (2010) show that in a low-NO_x environment, such as that of the Southern Hemisphere, differences in the isoprene oxidation scheme contribute considerably to the differences in the simulation of CO. They also study the isoprene oxidation mechanisms of the four models under consideration here, and rank them in terms of their production efficiency of CO from isoprene oxidation, with TM5 having highest conversion efficiency, CAM-chem the lowest, and GEOS-Chem and UKCA in between (e.g. Fig. 3 of Archibald et al., 2010). This corroborates with our finding that secondary CO dominates inter-model differences.

To further probe the differences between the models, we show vertical profiles of modelled key species, namely CO, HCHO, O_3, and OH mixing ratios, as well as the HO_2/OH ratio from each model in Fig. 14. We display data for January 2005 from the CLM-MEGANv2.1 simulation, because in austral summer the chemical production maximizes due to stronger photochemistry and higher biogenic emissions, and absolute inter-model differences in CO columns are also larger than in other seasons. TM5 is characterized by consistently high CO throughout the SH. However, TM5 also has the lowest HCHO, indicating that the photo-dissociation of HCHO may be somewhat high in that model. The CO values in NIWA-UKCA and in GEOS-Chem are very close in all three zones, exhibiting differences of ∼ 5–10 %, although CO in NIWA-UKCA is slightly higher than that in GEOS-Chem in the tropics but becomes lower towards remote regions. This may reflect slower meridional transport in NIWA-UKCA (shown in CO_{25}) combined with larger chemical production in the source region. The HCHO mixing ratios decrease sharply with altitude due to the dominant chemical precursors residing in the boundary layer and the efficient photo-dissociation, but the vertical gradient becomes smaller away from the source region, particularly in TM5, due to depletion of the biogenic precursor emissions in the remote SH. HCHO abundances in the four models correlate with OH to some extent, i.e. both OH and HCHO are relatively large in GEOS-Chem, whereas both are relatively small in TM5; this reflects the approximate linearity between the modelled HCHO abundance and methane oxidation via OH in the remote SH. However, there is no simple linear relationship between HCHO and OH; OH is involved in both the loss and the production of HCHO, and HCHO is one of the OH sources. The modelled OH profiles do not seem to be closely related to O_3 (the primary source of OH) in that TM5 has the lowest OH but its O_3 values lie in the middle of the model range. It is not clear if this is due to the difference in H_2O profiles in the meteorological datasets, or due to the differences in photolysis schemes. We also show HO_2 to OH ratios from each model; HO_2/OH is largest in TM5, indicating faster conversion of OH to HO_2 through $CO/CH_4/VOC$ oxidation processes in that model (or slower conversion of HO_2 to OH via NO_x-recycling, i.e. HO_2+NO reaction). Therefore,

from these comparisons it seems that the faster VOC photo-oxidation occurs in TM5 favouring enhanced CO production, together with the lower OH concentration (also shown in Table 1 in Fisher et al., 2014), leading to higher CO than in the other models.

5 Sensitivity of modelled SH CO and HCHO to uncertainties in biogenic emissions

In Sect. 3, we showed the model deviations in CO and HCHO columns from observed FTIR values at four remote SH sites using two different biogenic emissions inventories (for isoprene and monoterpenes), and find that modelled CO columns with LPJ-GUESS biogenic emissions are consistently lower and less representative of observed values than those produced using CLM-MEGANv2.1 emissions (Table 3). Here we further quantify the changes in CO and HCHO columns in response to changes in biogenic emissions at the hemispheric scale, and also highlight associated changes in the corresponding OH columns. Figures 15–17 display the monthly mean global distributions of relative differences in CO, HCHO, and OH columns between simulations using CLM-MEGANv2.1 and LPJ-GUESS, respectively, for January and July (averaged over 2004–2008). The differences calculated for all species are expressed as the percentage change relative to the CLM-MEGANv2.1 simulation. For all models, applying LPJ-GUESS emissions results in significant decreases in CO columns throughout the SH, with the largest decreases in the South American and Australian source regions (Fig. 15), in response to the smaller emission fluxes of isoprene and monoterpenes from LPJ-GUESS (the accumulated peak isoprene emissions in CLM-MEGANv2.1 are 25 % higher than in LPJ-GUESS during the peak season of the austral summer months, shown in Fig. 1, and the biggest differences are in South America). Away from these source regions, the differences are largely homogeneous in the mid- to high latitudes. The models' responses to changes in biogenic emissions vary considerably, with TM5 having the largest sensitivity of CO columns change to changes in biogenic emissions, namely ~ 35 % in January and ~ 25 % in July in the source regions and 10–15 % over

the remote SH. GEOS-Chem has the lowest sensitivity with 15–20 % changes in January and 10–15 % in July in the source reginos and less than 10 % in remote regions in response to the same emission changes of isoprene and monoterpenes. Note that for all models, the differences in CO columns due to changes in biogenic emissions in the source regions are larger in austral summer (January), but in remote regions, the larger changes occur in austral winter (July). This behaviour is probably attributable to annual variations in the regional CO lifetime which is reflected in OH changes shown in Fig. 17.

For corresponding changes in the tropospheric HCHO columns (Fig. 16), substantial decreases (up to ∼ 50–60 %) occur in the source regions of South America and Australia in response to smaller emission fluxes in LPJ-GUESS, relative to CLM-MEGANv2.1. The reduction in the HCHO columns propagates away from the sources to the sub-tropical remote oceans where the magnitude of the decreases is greatly reduced. There are some increases in HCHO columns over southern Africa, but decreases also occur; both of these are responses to the spatial variations of the biogenic emissions (also over Patagonia). However there is a consistent increase of up to 5 % over large areas of the mid- to high latitudes which is apparently not directly caused by reduced biogenic emissions. We find that changes in both CO and HCHO are associated with changes in OH (Fig. 17); the tropospheric OH columns have substantial increases in the source regions as a result of reduced isoprene and monoterpene emissions, and qualitatively these effects follow the differences in geographical distribution of the emissions, and are anti-correlated with both the CO and the HCHO columns changes there. OH changes in remote regions are largely positive, and are anti-correlated with the CO changes; i.e. through reduced CO loss rates leading to increases in OH. However increases in OH columns away from the sources are correlated with the HCHO changes; this implies that increases in HCHO in the remote region when applying LPJ-GUESS emissions are likely due to the increase in methane oxidation through the increase in OH. The inter-model differences in HCHO changes are generally small in the remote regions but TM5 shows the largest sensitivity over the

Title Page

Abstract | Introduction

Conclusions | References

Tables | Figures

|◄ | ►|

◄ | ►

Back | Close

Full Screen / Esc

Printer-friendly Version

Interactive Discussion

source region in both OH and HCHO, due primarily to the faster isoprene oxidation processes in that model. Note that the large relative differences in both HCHO and OH in July at high latitudes shown in CAM-chem are not significant because the background amounts of both species in the polar region are extremely low.

Complementing the comparison of columns, we here compare the seasonal differences in vertical profiles of CO mixing ratios between CLM-MEGANv2.1 and LPJ-GUESS simulations, averaged zonally and over 2004–2008. Figure 18 shows large reductions in CO over the SH tropics in all simulations using LPJ-GUESS emissions of isoprene and monoterpenes, relative to those using MEGANv2, and these reductions propagate to the upper SH tropical troposphere and spread throughout the middle and high latitudes. This shows that the CO column changes in the extratropics are dominated by the changes in the free and upper troposphere, where CO has a relatively long lifetime. Overall, the impact of biogenic emissions on CO are more significant in the SH than the NH.

6   Summary and conclusions

We have compared modelled daily-mean CO and HCHO columns from a four-model ensemble with the observed daily-mean FTIR columns of these two species at SH sites including the tropical site Darwin, mid-latitude sites Wollongong and Lauder, and the Antarctic site Arrival Heights for CO, and Wollongong and Lauder for HCHO. We use CLM-MEGANv2.1 biogenic emissions for the first set of simulations; for these simulations modelled and measured CO compare well, albeit with some low biases, in all models at all locations; annually averaged deviations relative to the observations are −3.2 % at Arrival Heights, −8.6 % at Lauder, −19.2 % at Wollongong, and −6.9 % at Darwin for the 4-model mean. The largest discrepancies between modelled and observed CO columns occur at Wollongong which is heavily influenced by local urban and industrial sources and episodic nearby bush fires that are most likely unaccounted for in the emission inventories. Large inter-model differences exist at all locations for

all seasons with the exception of austral spring at Darwin where the local biomass burning sources dominate the CO columns. We also compare the modelled surface CO to observations; significant inter-model differences exist although the ensemble mean exhibits good agreement with the observed values for most sites. The inter-model differences for modelled surface CO are significantly larger than the differences between modelled and observed surface CO. In agreement with previous modelling studies of HCHO in the remote SH, the models significantly underestimate observed HCHO columns at Wollongong and Lauder by more than a factor of 2, and the largest discrepancy occurs during austral summer. We cannot reconcile such significant differences between the modelled and observed HCHO columns over the remote SH with our current understanding and thus hypothesise that missing local sources and/or missing chemical processes are the most likely causes.

To determine the sensitivity of CO and HCHO distributions to biogenic emissions, we perform a second set of simulations with emissions of isoprene and monoterpene from the LPJ-GUESS dataset; results show that the LPJ-GUESS simulations exhibit systematically lower CO columns and lower surface CO than the CLM-MEGANv2.1 simulations. Annually averaged relative differences between ensemble model mean and observed CO columns are −10.5 % at Arrival Heights, −17.1 % at Lauder, −27.5 % at Wollongong, and −19.9 % at Darwin. The differences in surface CO between the two simulations are generally smaller than 5 %. We find that differences in biogenic emissions have no significant impact on modelled HCHO columns at neither Wollongong nor Lauder.

Examining the response of CO and HCHO columns to differences in biogenic emissions of isoprene and monoterpenes on the hemispheric scale, we show that both species exhibit large sensitivity to emissions in the source regions, with 30–40 % reduced CO and HCHO columns, as a direct consequence of the reduced emissions of isoprene and monoterpenes in the LPJ-GUESS inventory, relative to CLM-MEGAN v2.1, and these reductions are generally larger in summer than in winter. Inter-model differences exist regarding the sensitivity to changing the biogenic emissions, which

Full Screen / Esc

Printer-friendly Version

Interactive Discussion

can be attributed to the differences in isoprene and monoterpene oxidation processes between the models. Away from the source regions and throughout the SH, decreases in CO columns are roughly half those occurring in the source regions, whereas there are moderate increases in HCHO columns ($\sim 5\%$) despite the significant decreases in and near the source regions for all models. We show that the increases in HCHO columns in the remote SH for LPJ-GUESS, relative to CLM-MEGANv2.1, are linked to the increases in OH columns through enhanced methane oxidation in the remote SH. There are substantial increases in OH columns in the source regions in direct response to the reduced isoprene and monoterpene emissions in the LPJ-GUESS inventory, whereas the general increase (up to $\sim 5\%$ across the models) in the remote regions is the result of reductions in CO and possibly other longer-lived isoprene oxidation products.

Significant inter-model differences also exist in modelled CO columns; we quantify these differences in three latitudinal regions (SH tropics, mid-, and high latitudes). The ratios of individual model columns to the ensemble mean columns (annually averaged and averaged across the three regions) are between 0.85 and 1.15 for the tropical region, and the range increases to between 0.7 and 1.2 at high latitudes. Using diagnostic tracers, we assess the impact of modelled transport (by CO_{25}), the contribution from primarily-emitted CO (by CO_{OH}), and CO produced and transported from secondary CO production ($CO_{sec} = CO - CO_{OH}$). The results reveal that the differences in transport are not sufficient to explain the differences in modelled CO columns. The modelled range of CO_{OH} corresponds much better to the modelled CO columns than CO_{25} but still cannot fully explain the inter-model differences in modelled CO columns. The differences in secondary CO production, i.e. CO_{sec}, however, correspond well with those in modelled CO columns. TM5 exhibits the highest values in both variables, followed by GEOS-Chem, NIWA-UKCA, and CAM-chem in magnitude. We calculate that CO_{sec} contributes around 65% to CO in the tropics and around 75% in the polar region in each model, and is responsible for two thirds of the inter-model differences in modelled CO columns overall. This suggests that the models' differences in secondary

CO production from methane and NMVOCs oxidation play a major role in their ability to reproduce the CO columns in the SH, as also noted by Fisher et al. (2014).

We further examine the modelled vertical distribuitons of CO, HCHO, OH, O_3, and the HO_2/OH ratio. We find that inter-model variations in the distributions of these species do not follow simple patterns, suggesting that differences in the models' chemical mechanisms (including their photolysis schemes) might play an important role. Similarities in these variations are seen between CO and HCHO, O_3 and OH, and HCHO and OH. But one of the models, TM5, does not follow these patterns, e.g. it has the smallest HCHO columns but the largest CO, and also has the least OH despite O_3 values in the middle of the model range. HO_2/OH ratios are high in the SH due to the low-NO_x environment, and TM5 exhibits relatively higher HO_2/OH ratios across all regions, suggesting a faster conversion of OH to HO_2 leading to higher secondary CO formation rates from the oxidation of the VOCs. Note that TM5 employs a lumped chemical mechanism which contrasts with CAM-chem which is characterized by the most comprehensive mechanism of our ensemble, including more than 150 chemical species. In CAM-chem, this might result in a slower conversion rate of VOCs leading to secondary CO production, therefore the lowest CO columns compared to other models.

We conclude that the uncertainty in biogenic emissions remains a significant problem in modelling both long- and short-lived species throughout the SH. Given that the differences between the two biogenic emissions inventories used here are moderate compared to the much larger uncertainties existing in the current estimates of isoprene and monoterpenes emissions, the resultant uncertainty in modelled CO could be much larger. Although the ensemble model mean satisfactorily compares to observed CO in the SH, the large inter-model differences add more uncertainties in modelled CO and in constraining biogenic emissions. Note that in this paper, we do not separately quantify the effect from changes in monoterpene emissions. The emissions from monoterpene are around 30 and 10 % of those of isoprenes in CLM-MEGANv2.1 and LPJ-GUESS inventories, respectively, which could have a significant impact on modelled CO. How-

ever, due to the large uncertainty in emissions and the varying degrees of complexity of the monoterpene degradation schemes included in each model, this will further complicate the interpretation of the impact from changing monoterpene emissions.

References

Archibald, A., Jenkin, M., and Shallcross, D.: An isoprene mechanism intercomparison, Atmos. Environ., 44, 5356–5364, 2010. 2624, 2637, 2659

Arneth, A., Miller, P. A., Scholze, M., Hickler, T., Schurgers, G., Smith, B., and Prentice, I. C.: CO_2 inhibition of global terrestrial isoprene emissions: potential implications for atmospheric chemistry, Geophys. Res. Lett., 34, L18813, doi:10.1029/2007GL030615, 2007a. 2620, 2621

Arneth, A., Niinemets, Ü., Pressley, S., Bäck, J., Hari, P., Karl, T., Noe, S., Prentice, I. C., Serça, D., Hickler, T., Wolf, A., and Smith, B.: Process-based estimates of terrestrial ecosystem isoprene emissions: incorporating the effects of a direct CO_2-isoprene interaction, Atmos. Chem. Phys., 7, 31–53, doi:10.5194/acp-7-31-2007, 2007b. 2620

Arneth, A., Monson, R. K., Schurgers, G., Niinemets, Ü., and Palmer, P. I.: Why are estimates of global terrestrial isoprene emissions so similar (and why is this not so for monoterpenes)?, Atmos. Chem. Phys., 8, 4605–4620, doi:10.5194/acp-8-4605-2008, 2008. 2618

Arneth, A., Schurgers, G., Lathiere, J., Duhl, T., Beerling, D. J., Hewitt, C. N., Martin, M., and Guenther, A.: Global terrestrial isoprene emission models: sensitivity to variability in climate and vegetation, Atmos. Chem. Phys., 11, 8037–8052, doi:10.5194/acp-11-8037-2011, 2011. 2618

Arnold, S. R., Spracklen, D. V., Williams, J., Yassaa, N., Sciare, J., Bonsang, B., Gros, V., Peeken, I., Lewis, A. C., Alvain, S., and Moulin, C.: Evaluation of the global oceanic isoprene source and its impacts on marine organic carbon aerosol, Atmos. Chem. Phys., 9, 1253–1262, doi:10.5194/acp-9-1253-2009, 2009. 2633

Atkinson, R.: Atmospheric chemistry of VOCs and NO_x, Atmos. Environ., 34, 2063–2101, 2000. 2617

Atkinson, R., Baulch, D. L., Cox, R. A., Crowley, J. N., Hampson, R. F., Hynes, R. G., Jenkin, M. E., Rossi, M. J., Troe, J., and IUPAC Subcommittee: Evaluated kinetic and photochemical data for atmospheric chemistry: Volume II – gas phase reactions of organic species, Atmos. Chem. Phys., 6, 3625–4055, doi:10.5194/acp-6-3625-2006, 2006. 2633

Ayers, G. P., Gillett, R. W., Granek, H., de Serves, C., and Cox, R. A.: Formaldehyde production in clean marine air, Geophys. Res. Lett., 24, 401–404, 1997. 2632, 2633

Barkley, M. P., Palmer, P. I., Kuhn, U., Kesselmeier, J., Chance, K., Kurosu, T. P., Martin, R. V., Helmig, D., and Guenther, A.: Net ecosystem fluxes of isoprene over tropical South America inferred from Global Ozone Monitoring Experiment (GOME) observations of HCHO columns, J. Geophys. Res., 113, D20304, doi:10.1029/2008JD009863, 2008. 2618

Bey, I., Jacob, D. J., Yantosca, R. M., Logan, J. A., Field, B. D., Fiore, A. M., Li, Q. B., Liu, H. G. Y., Mickley, L. J., and Schultz, M. G.: Global modeling of tropospheric chemistry with assimilated meteorology: model description and evaluation, J. Geophys. Res., 106, 23073–23095, 2001. 2624

Bonsang, B., Polle, C., and Lambert, G.: Evidence for marine production of isoprene, Geophys. Res. Lett., 19, 1129–1132, 1992. 2633

Brasseur, G. P., Hauglustaine, D. A., Walters, S., and Rasch, P. J.: MOZART, a global chemical transport model for ozone and related chemical tracers, 1, Model description, J. Geophys. Res., 103, 28265–28289, 1998. 2623

DeCaria, A. J., Pickering, K. E., Stenchikov, G. L., and Ott, L. E.: Lightning-generated NO_x and its impact on tropospheric ozone production: a three-dimensional modeling study of a Stratosphere–Troposphere Experiment: Radiation, Aerosols and Ozone (STERAO-A) thunderstorm, J. Geophys. Res., 110, D14303, doi:10.1029/2004JD005556, 2006. 2626

Dee, D. P., Uppala, S. M., Simmons, A. J., Berrisford, P., Poli, P., Kobayashi, S., Andrae, U., Balmaseda, M. A., Balsamo, G., Bauer, P., Bechtold, P., Beljaars, A. C. M., van de Berg, L., Bidlot, J., Bormann, N., Delsol, C., Dragani, R., Fuentes, M., Geer, A. J., Haimberger, L., Healy, S. B., Hersbach, H., Hólm, E. V., Isaksen, L., Kållberg, P., Köhler, M., Matricardi, M., McNally, A. P., Monge-Sanz, B. M., Morcrette, J.-J., Park, B.-K., Peubey, C., de Rosnay, P., Tavolato, C., Thépaut, J.-N., and Vitart, F.: The ERA-Interim reanalysis: configuration and performance of the data assimilation system, Q. J. Roy. Meteor. Soc., 137, 553–597, 2011. 2623

de Laat, A. T. J., Gloudemans, A. M. S., Schrijver, H., Aben, I., Nagahama, Y., Suzuki, K., Mahieu, E., Jones, N. B., Paton-Walsh, C., Deutscher, N. M., Griffith, D. W. T., De Mazière, M., Mittermeier, R. L., Fast, H., Notholt, J., Palm, M., Hawat, T., Blumenstock, T., Hase, F., Schneider, M., Rinsland, C., Dzhola, A. V., Grechko, E. I., Poberovskii, A. M., Makarova, M. V., Mellqvist, J., Strandberg, A., Sussmann, R., Borsdorff, T., and Rettinger, M.: Validation of five years (2003–2007) of SCIAMACHY CO total column measurements using ground-based spectrometer observations, Atmos. Meas. Tech., 3, 1457–1471, doi:10.5194/amt-3-1457-2010, 2010. 2626, 2627

Deutscher, N. M., Griffith, D. W. T., Bryant, G. W., Wennberg, P. O., Toon, G. C., Washenfelder, R. A., Keppel-Aleks, G., Wunch, D., Yavin, Y., Allen, N. T., Blavier, J.-F., Jiménez, R., Daube, B. C., Bright, A. V., Matross, D. M., Wofsy, S. C., and Park, S.: Total column CO_2 measurements at Darwin, Australia – site description and calibration against in situ aircraft profiles, Atmos. Meas. Tech., 3, 947–958, doi:10.5194/amt-3-947-2010, 2010. 2626

Duncan, B. N., Logan, J. A., Bey, I., Megretskaia, I. A., Yantosca, R. M., Novelli, P. C., Jones, N. B., and Rinsland, C. P.: Global budget of CO, 1988–1997: source estimates and validation with a global model, J. Geophys. Res., 112, D22301, doi:10.1029/2007JD008459, 2007. 2617, 2618, 2624

Edwards, D. P., Emmons, L. K., Gille, J. C., Chu, A., Attié, J.-L., Giglio, L., Wood, S. W., Haywood, J., Deeter, M. N., Massie, S. T., Ziskin, D. C., and Drummond, J. R.: Satellite-observed pollution from Southern Hemisphere biomass burning, J. Geophys. Res., 111, D14312, doi:10.1029/2005JD006655, 2006. 2617

Emmons, L. K., Walters, S., Hess, P. G., Lamarque, J.-F., Pfister, G. G., Fillmore, D., Granier, C., Guenther, A., Kinnison, D., Laepple, T., Orlando, J., Tie, X., Tyndall, G., Wiedinmyer, C., Baughcum, S. L., and Kloster, S.: Description and evaluation of the Model for Ozone

Title Page

Abstract | Introduction

Conclusions | References

Tables | Figures

◄◄ | ►►

◄ | ►

Back | Close

Full Screen / Esc

Printer-friendly Version

Interactive Discussion

and Related chemical Tracers, version 4 (MOZART-4), Geosci. Model Dev., 3, 43–67, doi:10.5194/gmd-3-43-2010, 2010. 2625, 2659

Eyring, V., Lamarque, J.-F., Hess, P., Arfeuille, F., Bowman, K., Chipperfield, M. P., Duncan, B., Fiore, A., Gettelman, A., Giorgetta, M. A., Granier, C., Hegglin, M., Kinnison, D., Kunze, M., Langematz, U., Luo, B., Martin, R., Matthes, K., Newman, P. A., Peter, T., Robock, A., Ryerson, T., Saiz-Lopez, A., Salawitch, R., Schultz, M., Shepherd, T. G., Shindell, D., Stähelin, J., Tegtmeier, S., Thomason, L., Tilmes, S., Vernier, J.-P., Waugh, D. W., and Young, P. J.: Overview of IGAC/SPARC Chemistry–Climate Model Initiative (CCMI) community simulations in support of upcoming ozone and climate assessments, SPARC Newsletter, 40, 48–66, 2013. 2625

Fisher, J. A., Jacob, D. J., Purdy, M. T., Kopacz, M., Le Sager, P., Carouge, C., Holmes, C. D., Yantosca, R. M., Batchelor, R. L., Strong, K., Diskin, G. S., Fuelberg, H. E., Holloway, J. S., Hyer, E. J., McMillan, W. W., Warner, J., Streets, D. G., Zhang, Q., Wang, Y., and Wu, S.: Source attribution and interannual variability of Arctic pollution in spring constrained by aircraft (ARCTAS, ARCPAC) and satellite (AIRS) observations of carbon monoxide, Atmos. Chem. Phys., 10, 977–996, doi:10.5194/acp-10-977-2010, 2010. 2617

Fisher, J. A., Wilson, S. R., Zeng, G., Williams, J. E., Emmons, L. K., Langenfelds, R. L., Krummel, P. B., and Steele, L. P.: Seasonal changes in the tropospheric carbon monoxide profile over the remote Southern Hemisphere evaluated using multi-model simulations and aircraft observations, Atmos. Chem. Phys. Discuss., 14, 27531–27578, doi:10.5194/acpd-14-27531-2014, 2014. 2619, 2629

Fishman, J., Fakhruzzaman, K., Cros, B., and Nganga, D.: Identification of widespread pollution in the Southern Hemisphere deduced from satellite analyses, Science, 252, 1693–1696, 1991. 2617

Gloudemans, A. M. S., Krol, M. C., Meirink, J. F., de Laat, A. T. J., van der Werf, G. R., Schrijver, H., van den Broek, M. M. P., and Aben, I.: Evidence for long-range transport of carbon monoxide in the Southern Hemisphere from SCIAMACHY observations, Geophys. Res. Lett., 33, L16807, doi:10.1029/2006GL026804, 2006. 2617

Granier, C., Bessagnet, B., Bond, T., D'Angiola, A., Denier van der Gon, H., Frost, G. J., Heil, A., Kaiser, J. W., Kinne, S., Klimont, Z., Kloster, S.-F., Lamarque, J., Liousse, C., Masui, T., Meleux, F., Mieville, A., Ohara, T., Raut, J.-C., Riahi, K., Schultz, M. G., Smith, S. J., Thompson, A., van Aardenne, J., van der Werf, G. R., and van Vuuren, D. P.: Evolution of anthropogenic and biomass burning emissions of air pollutants at global and regional scales during

the 1980–2010 period, Climatic Change, 109, 163–190, doi:10.1007/s10584-011-0154-1, 2011. 2621

Guenther, A. B., Jiang, X., Heald, C. L., Sakulyanontvittaya, T., Duhl, T., Emmons, L. K., and Wang, X.: The Model of Emissions of Gases and Aerosols from Nature version 2.1 (MEGAN2.1): an extended and updated framework for modeling biogenic emissions, Geosci. Model Dev., 5, 1471–1492, doi:10.5194/gmd-5-1471-2012, 2012. 2618, 2620, 2621

Heald, C. L., Jacob, D. J., Fiore, A. M., Emmons, L. K., Gille, J. C., Deeter, M. N., Warner, J., Edwards, D. P., Crawford, J. H., Hamlin, A. J., Sachse, G. W., Browell, E. V., Avery, M. A., Vay, S. A., Westberg, D. J., Blake, D. R., Singh, H. B., Sandholm, S. T., Talbot, R. W., and Fuelberg, H. E.: Asian outflow and transpacific transport of carbon monoxide and ozone pollution: an integrated satellite, aircraft and model perspective, J. Geophys. Res., 108, 4804, doi:10.1029/2003JD003507, 2003. 2617

Hewitt, H. T., Copsey, D., Culverwell, I. D., Harris, C. M., Hill, R. S. R., Keen, A. B., McLaren, A. J., and Hunke, E. C.: Design and implementation of the infrastructure of HadGEM3: the next-generation Met Office climate modelling system, Geosci. Model Dev., 4, 223–253, doi:10.5194/gmd-4-223-2011, 2011. 2622

Holloway, T., Levy II, H., and Kasibhatla, P.: Global distribution of carbon monoxide, J. Geophys. Res., 105, 12123–12147, doi:10.1029/1999JD901173, 2000. 2618

Huijnen, V., Williams, J., van Weele, M., van Noije, T., Krol, M., Dentener, F., Segers, A., Houweling, S., Peters, W., de Laat, J., Boersma, F., Bergamaschi, P., van Velthoven, P., Le Sager, P., Eskes, H., Alkemade, F., Scheele, R., Nédélec, P., and Pätz, H.-W.: The global chemistry transport model TM5: description and evaluation of the tropospheric chemistry version 3.0, Geosci. Model Dev., 3, 445–473, doi:10.5194/gmd-3-445-2010, 2010. 2623

Jacob, D. J., Field, B. D., Jin, E. M., Bey, I., Li, Q., Logan, J. A., Yantosca, R. M., and Singh. H. B.: Atmospheric budget of acetone, J. Geophys. Res., 107, ACH 5-1–ACH 5-17, doi:10.1029/2001JD000694, 2002. 2624

Jones, N. B., Rinsland, C. P., Liley, J. B., and Rosen, J.: Correlation of aerosol and carbon monoxide at 45° S: evidence of biomass burning emissions, Geophys. Res. Lett., 28, 709–712, 2001. 2626

Jones, N. B., Riedel, K., Allan, W., Wood, S., Palmer, P. I., Chance, K., and Notholt, J.: Long-term tropospheric formaldehyde concentrations deduced from ground-based fourier transform solar infrared measurements, Atmos. Chem. Phys., 9, 7131–7142, doi:10.5194/acp-9-7131-2009, 2009. 2619, 2626, 2627, 2633, 2634

Kurokawa, J., Ohara, T., Morikawa, T., Hanayama, S., Janssens-Maenhout, G., Fukui, T., Kawashima, K., and Akimoto, H.: Emissions of air pollutants and greenhouse gases over Asian regions during 2000–2008: Regional Emission inventory in ASia (REAS) version 2, Atmos. Chem. Phys., 13, 11019–11058, doi:10.5194/acp-13-11019-2013, 2013. 2621

Lamarque, J.-F., Bond, T. C., Eyring, V., Granier, C., Heil, A., Klimont, Z., Lee, D., Liousse, C., Mieville, A., Owen, B., Schultz, M. G., Shindell, D., Smith, S. J., Stehfest, E., Van Aardenne, J., Cooper, O. R., Kainuma, M., Mahowald, N., McConnell, J. R., Naik, V., Riahi, K., and van Vuuren, D. P.: Historical (1850–2000) gridded anthropogenic and biomass burning emissions of reactive gases and aerosols: methodology and application, Atmos. Chem. Phys., 10, 7017–7039, doi:10.5194/acp-10-7017-2010, 2010. 2621

Lamarque, J.-F., Emmons, L. K., Hess, P. G., Kinnison, D. E., Tilmes, S., Vitt, F., Heald, C. L., Holland, E. A., Lauritzen, P. H., Neu, J., Orlando, J. J., Rasch, P. J., and Tyndall, G. K.: CAM-chem: description and evaluation of interactive atmospheric chemistry in the Community Earth System Model, Geosci. Model Dev., 5, 369–411, doi:10.5194/gmd-5-369-2012, 2012. 2625

Langenfelds, R., Francey, R., Steele, L., Fraser, P., Coram, S., Hayes, M., Beardsmore, D., Lucarelli, M., and deSilva, F.: Improved vertical sampling of the trace gas composition of the troposphere above Cape Grim since 1991, in: Baseline Atmospheric Program (Australia) 15 1993, edited by: Francey, R., Dick, A., and Derek, N., Bureau of Meteorology and CSIRO Division of Atmospheric Research, Melbourne, Australia, 45–56, 1996. 2619

Lawrence, D. M., Oleson, K. W., Flanner, M. G., Thorton, P. E., Swenson, S. C., Lawrence, P. J., Zeng, X., Yang, Z.-L., Levis, S., Skaguchi, K., Bonan, G. B., and Slater, A. G.: Parameterization improvements and functional and structural advances in version 4 of the Community Land Model, J. Adv. Model. Earth Sys., 3, M03001, doi:10.1029/2011ms000045, 2011. 2621

Lawson, S. J., Selleck, P. W., Galbally, I. E., Keywood, M. D., Harvey, M. J., Lerot, C., Helmig, D., and Ristovski, Z.: Seasonal in situ observations of glyoxal and methylglyoxal over the temperate oceans of the Southern Hemisphere, Atmos. Chem. Phys. Discuss., 14, 21659–21708, doi:10.5194/acpd-14-21659-2014, 2014. 2633

Levy II, H.: Normal atmosphere: large radical and formaldehyde concentrations predicted, Science, 173, 141–143, 1971. 2617

Liang, Q., Jaegle, L., Jaffe, D. A., Weiss, P., Heckman, A., and Snow, J.: Long-range transport to the Northeast Pacific: seasonal variations and transport pathways, J. Geophys. Res., 109, D23S07, doi:10.1029/2003JD004402, 2004. 2617

Mao, J., Jacob, D. J., Evans, M. J., Olson, J. R., Ren, X., Brune, W. H., Clair, J. M. St., Crounse, J. D., Spencer, K. M., Beaver, M. R., Wennberg, P. O., Cubison, M. J., Jimenez, J. L., Fried, A., Weibring, P., Walega, J. G., Hall, S. R., Weinheimer, A. J., Cohen, R. C., Chen, G., Crawford, J. H., McNaughton, C., Clarke, A. D., Jaeglé, L., Fisher, J. A., Yantosca, R. M., Le Sager, P., and Carouge, C.: Chemistry of hydrogen oxide radicals (HO_x) in the Arctic troposphere in spring, Atmos. Chem. Phys., 10, 5823–5838, doi:10.5194/acp-10-5823-2010, 2010. 2625

Mao, J., Paulot, F., Jacob, D. J., Cohen, R. C., Crounse, J. D., Wennberg, P. O., Keller, C. A., Hudman, R. C., Barkley, M. P., and Horowitz, L. W.: Ozone and organic nitrates over the eastern United States: sensitivity to isoprene chemistry, J. Geophys. Res., 118, 11256–11268, doi:10.1002/jgrd.50817, 2013a. 2625

Mao, J., Fan, S., Jacob, D. J., and Travis, K. R.: Radical loss in the atmosphere from Cu-Fe redox coupling in aerosols, Atmos. Chem. Phys., 13, 509–519, doi:10.5194/acp-13-509-2013, 2013b. 2625

Marais, E. A., Jacob, D. J., Guenther, A., Chance, K., Kurosu, T. P., Murphy, J. G., Reeves, C. E., and Pye, H. O. T.: Improved model of isoprene emissions in Africa using Ozone Monitoring Instrument (OMI) satellite observations of formaldehyde: implications for oxidants and particulate matter, Atmos. Chem. Phys., 14, 7693–7703, doi:10.5194/acp-14-7693-2014, 2014. 2618

McLinden, C. A., Olsen, S. C., Hannegan, B., Wild, O., Prather, M. J., and Sundet, J.: Stratospheric ozone in 3-D models: a simple chemistry and the cross-tropopause flux, J. Geophys. Res., 105, 14653–14665, 2000. 2624

Meinshausen, M., Smith, S. J., Calvin, K., Daniel, J. S., Kainuma, M. L. T., Lamarque, J.-F., Matsumoto, K., Montzka, S. A., Raper, S. C. B., Riahi, K., Thomson, A., Velders, G. J. M., and van Vuuren, D. P. P.: The RCP greenhouse gas concentrations and their extensions from 1765 to 2300, Climatic Change, 109, 213–241, doi:10.1007/s10584-011-0156-z, 2011. 2626

Mickley, L. J., Jacob, D. J., and Rind, D.: Uncertainty in preindustrial abundance of tropospheric ozone: implications for radiative forcing calculations, J. Geophys. Res., 106, 3389–3399, 2000.

Millet, D. B., Jacob, D. J., Custer, T. G., de Gouw, J. A., Goldstein, A. H., Karl, T., Singh, H. B., Sive, B. C., Talbot, R. W., Warneke, C., and Williams, J.: New constraints on terrestrial and oceanic sources of atmospheric methanol, Atmos. Chem. Phys., 8, 6887–6905, doi:10.5194/acp-8-6887-2008, 2008. 2625

Morgenstern, O., Braesicke, P., O'Connor, F. M., Bushell, A. C., Johnson, C. E., Osprey, S. M., and Pyle, J. A.: Evaluation of the new UKCA climate-composition model – Part 1: The stratosphere, Geosci. Model Dev., 2, 43–57, doi:10.5194/gmd-2-43-2009, 2009. 2622

Morgenstern, O., Zeng, G., Wood, S. W. W., Robinson, J., Smale, D., Paton-Walsh, C., Jones, N. B., and Griffith, D. W. T.: Long-range correlations in Fourier transform infrared, satellite, and modeled CO in the Southern Hemisphere, J. Geophys. Res., 117, D11301, doi:10.1029/2012JD017639, 2012. 2617, 2619, 2626

Morgenstern, O., Zeng, G., Luke Abraham, N., Telford, P. J., Braesicke, P., Pyle, J. A., Hardiman, S. C., O'Connor, F. M., and Johnson, C. E.: Impacts of climate change, ozone recovery, and increasing methane on surface ozone and the tropospheric oxidizing capacity, J. Geophys. Res., 118, 1028–1041, doi:10.1029/2012JD018382, 2013. 2622, 2623

Murray, L. T., Jacob, D. J., Logan, J. A., Hudman, R. C., and Koshak, W. J.: Optimized regional and interannual variability of lightning in a global chemical transport model constrained by LIS/OTD satellite data, J. Geophys. Res., 117, D20307, doi:10.1029/2012JD017934, 2012. 2625

Murray, L. T., Logan, J. A., and Jacob, D. J.: Interannual variability in tropical tropospheric ozone and OH: the role of lightning, J. Geophys. Res., 118, 11,468–11,480, doi:10.1002/jgrd.50857, 2013. 2624

Naik, V., Voulgarakis, A., Fiore, A. M., Horowitz, L. W., Lamarque, J.-F., Lin, M., Prather, M. J., Young, P. J., Bergmann, D., Cameron-Smith, P. J., Cionni, I., Collins, W. J., Dalsøren, S. B., Doherty, R., Eyring, V., Faluvegi, G., Folberth, G. A., Josse, B., Lee, Y. H., MacKenzie, I. A., Nagashima, T., van Noije, T. P. C., Plummer, D. A., Righi, M., Rumbold, S. T., Skeie, R., Shindell, D. T., Stevenson, D. S., Strode, S., Sudo, K., Szopa, S., and Zeng, G.: Preindustrial to present-day changes in tropospheric hydroxyl radical and methane lifetime from the Atmospheric Chemistry and Climate Model Intercomparison Project (ACCMIP), Atmos. Chem. Phys., 13, 5277–5298, doi:10.5194/acp-13-5277-2013, 2013. 2618

Novelli, P. C., Masarie, K. A., and Lang, P. M.: Distributions and recent changes of carbon monoxide in the lower troposphere, J. Geophys. Res., 103, 19015–19034, 1998. 2627

O'Connor, F. M., Johnson, C. E., Morgenstern, O., Abraham, N. L., Braesicke, P., Dalvi, M., Folberth, G. A., Sanderson, M. G., Telford, P. J., Voulgarakis, A., Young, P. J., Zeng, G., Collins, W. J., and Pyle, J. A.: Evaluation of the new UKCA climate-composition model – Part 2: The Troposphere, Geosci. Model Dev., 7, 41–91, doi:10.5194/gmd-7-41-2014, 2014. 2622

Title Page

Abstract	Introduction
Conclusions	References
Tables	Figures

|◄ | ►|

◄ | ►

Back | Close

Full Screen / Esc

Printer-friendly Version

Interactive Discussion

Ohara, T., Akimoto, H., Kurokawa, J., Horii, N., Yamaji, K., Yan, X., and Hayasaka, T.: An Asian emission inventory of anthropogenic emission sources for the period 1980–2020, Atmos. Chem. Phys., 7, 4419–4444, doi:10.5194/acp-7-4419-2007, 2007.

Palmer, P. I., Jacob, D. J., Fiore, A. M., Martin, R. V., Chance, K., and Kurosu, T. P.: Mapping isoprene emissions over North America using formaldehyde column observations from space, J. Geophys. Res., 108, 4180, doi:10.1029/2002JD002153, 2003. 2618

Paton-Walsh, C., Deutscher, N. M., Griffith, D. W. T., Forgan, B. W., Wilson, S. R., Jones, N. B., and Edwards, D. P.: Trace gas emissions from savanna fires in northern Australia, J. Geophys. Res., 115, D16314, doi:10.1029/2009JD013309, 2010. 2626

Paulot, F., Crounse, J. D., Kjaergaard, H. G., Kroll, J. H., Seinfeld, J. H., and Wennberg, P. O.: Isoprene photooxidation: new insights into the production of acids and organic nitrates, Atmos. Chem. Phys., 9, 1479–1501, doi:10.5194/acp-9-1479-2009, 2009a. 2623, 2624, 2659

Paulot, F., Crounse, J. D., Kjaergaard, H. G., Kürten, A., Clair, J. M. S., Seinfeld, J. H., and Wennberg, P. O.: Unexpected epoxide formation in the gas-phase photooxidation of isoprene, Science, 325, 730–733, 2009b. 2623, 2624, 2659

Pfister, G. G., Emmons, L. K., Hess, P. G., Lamarque, J.-F., Orlando, J. J., Walters, S., Guenther, A., Palmer, P. I., and Lawrence, P. J.: Contribution of isoprene to chemical budgets: a model tracer study with the NCAR CTM MOZART-4, J. Geophys. Res., 113, D05308, doi:10.1029/2007JD008948, 2008. 2617, 2637

Pöschl, U., von Kuhlmann, R., Poisson, N., and Crutzen, P.: Development and intercomparison of condensed isoprene oxidation mechanisms for global atmospheric modeling, J. Atmos. Chem., 37, 29–52, doi:10.1023/A:1006391009798, 2000. 2659

Price, C. and Rind, D.: A simple lightning parameterization for calculating global lightning distributions, J. Geophys. Res., 97, 9919–9933, 1992. 2623, 2624, 2626

Price, C. and Rind, D.: Modeling global lightning distributions in a general-circulation model, Mon. Weather Rev., 122, 1930–1939, 1994.

Price, C., Penner, J., and Prather, M.: NO_x from lightning. 2. Constraints from the global atmospheric electric circuit, J. Geophys. Res., 102, 5943–5951, doi:10.1029/96JD02551, 1997. 2626

Ridley, B., Pickering, K., and Dye, J.: Comments on the parameterization of lightning-produced NO in global chemistry-transport models, Atmos. Environ., 39, 6184–6187, 2005. 2626

Rinsland, C. P., Jones, N. B., Connor, B. J., Logan, J. A., Pougatchev, N. S., Goldman, A., Murcray, F. J., Stephen, M., Pine, A. S., Zander, R., Mahieu, E., and Demoulin, P.: Northern and

Title Page

Abstract | Introduction

Conclusions | References

Tables | Figures

|◄ | ►|

◄ | ►

Back | Close

Full Screen / Esc

Printer-friendly Version

Interactive Discussion

Southern Hemisphere ground-based infrared spectroscopic measurements of tropospheric carbon monoxide and ethane, J. Geophys. Res., 103, 28197–28217, 1998. 2626

Rinsland, C. P., Jones, N. B., Connor, B. J., Wood, S. W., Goldman, A., Stephen, T. M., Murcray, F. J., Chiou, L. S., Zander, R., and Mahieu, E.: Multiyear infrared solar spectroscopic measurements of HCN, CO, C_2H_6, and C_2H_2 tropospheric columns above Lauder, New Zealand (45° S latitude), J. Geophys. Res., 107, ACH 1-1–ACH 1-12, doi:10.1029/2001JD001150, 2002. 2626

Rinsland, C. P., Dufour, G., Boone, C. D., Bernath, P. F., and Chiou, L.: Atmospheric Chemistry Experiment (ACE) measurements of elevated Southern Hemisphere upper tropospheric CO, C_2H_6, HCN, and C_2H_2 mixing ratios from biomass burning emissions and long-range transport, Geophys. Res. Lett., 32, L20803, doi:10.1029/2005GL024214, 2005. 2617

Schurgers, G., Arneth, A., Holzinger, R., and Goldstein, A. H.: Process-based modelling of biogenic monoterpene emissions combining production and release from storage, Atmos. Chem. Phys., 9, 3409–3423, doi:10.5194/acp-9-3409-2009, 2009. 2620, 2621

Shim, C., Wang, Y., Choi, Y., Palmer, P. I., Abbot, D. S., and Chance, K.: Constraining global isoprene emissions with Global Ozone Monitoring Experiment (GOME) formaldehyde column measurements, J. Geophys. Res., 110, D24301, doi:10.1029/2004JD005629, 2005. 2618

Shindell, D. T., Faluvegi, G., Stevenson, D. S., Krol, M. C., Emmons, L. K., Lamarque, J.-F., Petron, G., Dentener, F. J., Ellingsen, K., Schultz, M. G., Wild, O., Amann, M., Atherton, C. S., Bergmann, D. J., Bey, I., Butler, T., Cofala, J., Collins, W. J., Derwent, R. G., Doherty, R. M., Drevet, J., Eskes, H. J., Fiore, A. M., Gauss, M., Hauglustaine, D. A., Horowitz, L. W., Isaksen, I. S. A., Lawrence, M. G., Montanaro, V., Muller, J. F., Pitari, G., Prather, M. J., Pyle, J. A., Rast, S., Rodriguez, J. M., Sanderson, M. G., Savage, N. H., Strahan, S. E., Sudo, K., Szopa, S., Unger, N., van Noije, T. P. C., and Zeng, G.: Multi-model simulations of carbon monoxide: comparison with observations and projected near-future changes, J. Geophys. Res., 111, D19306, doi:10.1029/2006JD007100, 2006. 2618

Staudt, A., Jacob, D., Logan, J., Bachiochi, D., Krishnamurti, T., and Sachse, G.: Continental sources, transoceanic transport, and interhemispheric exchange of carbon monoxide over the Pacific, J. Geophys. Res., 106, 32571–32589, 2001. 2617

Stein, O., Schultz, M. G., Bouarar, I., Clark, H., Huijnen, V., Gaudel, A., George, M., and Clerbaux, C.: On the wintertime low bias of Northern Hemisphere carbon monoxide found in global model simulations, Atmos. Chem. Phys., 14, 9295–9316, doi:10.5194/acp-14-9295-2014, 2014. 2618

Title Page

Abstract | Introduction

Conclusions | References

Tables | Figures

|◄ | ►|

◄ | ►

Back | Close

Full Screen / Esc

Printer-friendly Version

Interactive Discussion

Stevenson, D. S., Dentener, F. J., Schultz, M. G., Ellingsen, K., van Noije, T. P. C., Wild, O., Zeng, G., Amann, M., Atherton, C. S., Bell, N., Bergmann, D. J., Bey, I., Butler, T., Cofala, J., Collins, W. J., Derwent, R. G., Doherty, R. M., Drevet, J., Eskes, H. J., Fiore, A. M., Gauss, M., Hauglustaine, D. A., Horowitz, L. W., Isaksen, I. S. A., Krol, M. C., Lamarque, J.-F., Lawrence, M. G., Montanaro, V., Muller, J.-F., Pitari, G., Prather, M. J., Pyle, J. A., Rast, S., Rodriguez, J. M., Sanderson, M. G., Savage, N. H., Shindell, D. T., Strahan, S. E., Sudo, K., and Szopa, S.: Multimodel ensemble simulations of present-day and near-future tropospheric ozone, J. Geophys. Res., 111, D08301, doi:10.1029/2005JD006338, 2006. 2618

Swinnerton, J. W., Linnenbom, V. J., and Lamontagne, R. A.: The ocean: a natural source of carbon monoxide, Science, 167, 984–986, 1970. 2617

van der Werf, G. R., Randerson, J. T., Giglio, L., Collatz, G. J., Mu, M., Kasibhatla, P. S., Morton, D. C., DeFries, R. S., Jin, Y., and van Leeuwen, T. T.: Global fire emissions and the contribution of deforestation, savanna, forest, agricultural, and peat fires (1997–2009), Atmos. Chem. Phys., 10, 11707–11735, doi:10.5194/acp-10-11707-2010, 2010. 2621

Velazco, V., Wood, S. W., Sinnhuber, M., Kramer, I., Jones, N. B., Kasai, Y., Notholt, J., Warneke, T., Blumenstock, T., Hase, F., Murcray, F. J., and Schrems, O.: Annual variation of strato-mesospheric carbon monoxide measured by ground-based Fourier transform infrared spectrometry, Atmos. Chem. Phys., 7, 1305–1312, doi:10.5194/acp-7-1305-2007, 2007. 2628

Vigouroux, C., Hendrick, F., Stavrakou, T., Dils, B., De Smedt, I., Hermans, C., Merlaud, A., Scolas, F., Senten, C., Vanhaelewyn, G., Fally, S., Carleer, M., Metzger, J.-M., Müller, J.-F., Van Roozendael, M., and De Mazière, M.: Ground-based FTIR and MAX-DOAS observations of formaldehyde at Réunion Island and comparisons with satellite and model data, Atmos. Chem. Phys., 9, 9523–9544, doi:10.5194/acp-9-9523-2009, 2009. 2619, 2633, 2634

Wai, K. M., Wu, S., Kumar, A., and Liao, H.: Seasonal variability and long-term evolution of tropospheric composition in the tropics and Southern Hemisphere, Atmos. Chem. Phys., 14, 4859–4874, doi:10.5194/acp-14-4859-2014, 2014. 2630

Washenfelder, R. A., Toon, G. C., Blavier, J.-F., Yang, Z., Allen, N. T., Wennberg, P. O., Vay, S. A., Matross, D. M., and Daube, B. C.: Carbon dioxide column abundances at the Wisconsin Tall Tower site, J. Geophys. Res., 111, D22305, doi:10.1029/2006JD007154, 2006. 2626

Watson, C. E., Fishman, J., and Reichle Jr., H. G.: The significance of biomass burning as a source of carbon monoxide and ozone in the Southern Hemisphere tropics: a satellite analysis, J. Geophys. Res., 95, 16443–16450, 1990. 2617

Title Page

Abstract | Introduction

Conclusions | References

Tables | Figures

|◄ | ►|

◄ | ►

Back | Close

Full Screen / Esc

Printer-friendly Version

Interactive Discussion

Wells, K. C., Millet, D. B., Cady-Pereira, K. E., Shephard, M. W., Henze, D. K., Bousserez, N., Apel, E. C., de Gouw, J., Warneke, C., and Singh, H. B.: Quantifying global terrestrial methanol emissions using observations from the TES satellite sensor, Atmos. Chem. Phys., 14, 2555–2570, doi:10.5194/acp-14-2555-2014, 2014. 2632

5 Wesely, M. L.: Parameterization of surface resistances to gaseous dry deposition in regional-scale numerical models, Atmos. Environ., 23, 1293–1304, 1989. 2622

Williams, J. E., van Weele, M., van Velthoven, P. F. J., Scheele, M. P., Liousse, C., and van der Werf, G. R.: The impact of uncertainties in african biomass burning emission estimates on modeling global air quality, long range transport and tropospheric chemical lifetimes, Atmo-
10 sphere, 3, 132–163, 2012. 2630

Williams, J. E., van Velthoven, P. F. J., and Brenninkmeijer, C. A. M.: Quantifying the uncertainty in simulating global tropospheric composition due to the variability in global emission estimates of Biogenic Volatile Organic Compounds, Atmos. Chem. Phys., 13, 2857–2891, doi:10.5194/acp-13-2857-2013, 2013. 2623, 2624

15 Williams, J. E., Le Bras, G., Kukui, A., Ziereis, H., and Brenninkmeijer, C. A. M.: The impact of the chemical production of methyl nitrate from the $NO + CH_3O_2$ reaction on the global distributions of alkyl nitrates, nitrogen oxides and tropospheric ozone: a global modelling study, Atmos. Chem. Phys., 14, 2363–2382, doi:10.5194/acp-14-2363-2014, 2014. 2623

Williamson, G. J., Price, O. F., Henderson, S. B., and Bowman, D. M. J. S.: Satellite-based
20 comparison of fire intensity and smoke plumes from prescribed fires and wildfires in southeastern Australia, Int. J. Wildland Fire, 22, 121–129, 2013. 2632

Wunch, D., Toon, G. C., Blavier, J.-F., Washenfelder, R. A., Notholt, J., Connor, B., Griffith, D. W. T., Sherlock, V., and Wennberg, P. O.: The Total Carbon Column Observing Network (TCCON), Philos. T. R. Soc. A, 369, 2087–2112 doi:10.1098/rsta.2010.0240, 2011.
25 2626

Yarwood, G., Rao, S., Yocke, M., and Whitten, G.: Updates to the carbon bond chemical mechanism: CB05, Final report to the US EPA, EPA Report Number: RT-0400675, available at: www.camx.com, 2005. 2624, 2659

Zeng, G., Pyle, J. A., and Young, P. J.: Impact of climate change on tropospheric ozone and its
30 global budgets, Atmos. Chem. Phys., 8, 369–387, doi:10.5194/acp-8-369-2008, 2008. 2623

Zeng, G., Wood, S. W., Morgenstern, O., Jones, N. B., Robinson, J., and Smale, D.: Trends and variations in CO, C_2H_6, and HCN in the Southern Hemisphere point to the declining anthro-

pogenic emissions of CO and C_2H_6, Atmos. Chem. Phys., 12, 7543–7555, doi:10.5194/acp-12-7543-2012, 2012. 2626, 2627

Table 1. Yearly total surface emissions ($Tg\,yr^{-1}$). Values in brackets are sums of SH emissions.

	2004	2005	2006	2007	2008	Mean
NO	84	87	87	89	87	87
CO	973	1003	1035	1001	950	992
C_5H_8 (**M**)	508 (269)	463 (246)	462 (243)	481 (254)	494 (265)	482 (255)
C_5H_8 (**G**)	442 (212)	450 (220)	433 (205)	439 (210)	431 (207)	439 (211)
$C_{10}H_{16}$ (**M**)	143 (72)	132 (66)	132 (68)	138 (70)	136 (68)	136 (69)
$C_{10}H_{16}$ (**G**)	35 (11)	36 (12)	34 (11)	35 (11)	34 (11)	35 (11)

M denotes CLM-MEGANv2.1 emissions; **G** denotes LPJ-GUESS emissions.

Table 2. Summary of model information.

	Resolution (lon/lat/lev)	Meteorology	Chemistry	Isoprene oxidation scheme
NIWA-UKCA **CCM**	$3.75°/2.5°/60$	Driven by observed SSTs and sea ice	Strat.+Trop. chemistry, 85 species	Mainz Isoprene Mechanism; Pöschl et al. (2000), updated rates; Paulot et al. (2009a, b)
TM5 **CTM**	$3.0°/2.0°/34$	ERA-interim	Modified CB05, 60 species	CB05; Yarwood et al. (2005), modified HO_2 yields; Archibald et al. (2010)
GEOS-Chem **CTM**	$2.5°/2.0°/47$	GEOS-5	Trop. chemistry, 121 species; 106 transported	Caltech Isoprene Mechanism; Paulot et al. (2009a, b)
CAM-Chem **CCM**	$2.5°/1.9°/56$	Specified dynamics, MERRA reanalysis	Strat.+Trop. chemistry 150 species	MOZART scheme; Emmons et al. (2010)

Table 3. Multi-annual mean averaged ensemble model mean deviations (%) from observed FTIR CO columns.

	CLM-MEGANv2.1	LPJ-GUESS
Arrival Heights	−3.2 %	−10.5 %
Lauder	−8.6 %	−17.1 %
Wollongong	−19.2 %	−27.5 %
Darwin	−6.9 %	−19.9 %
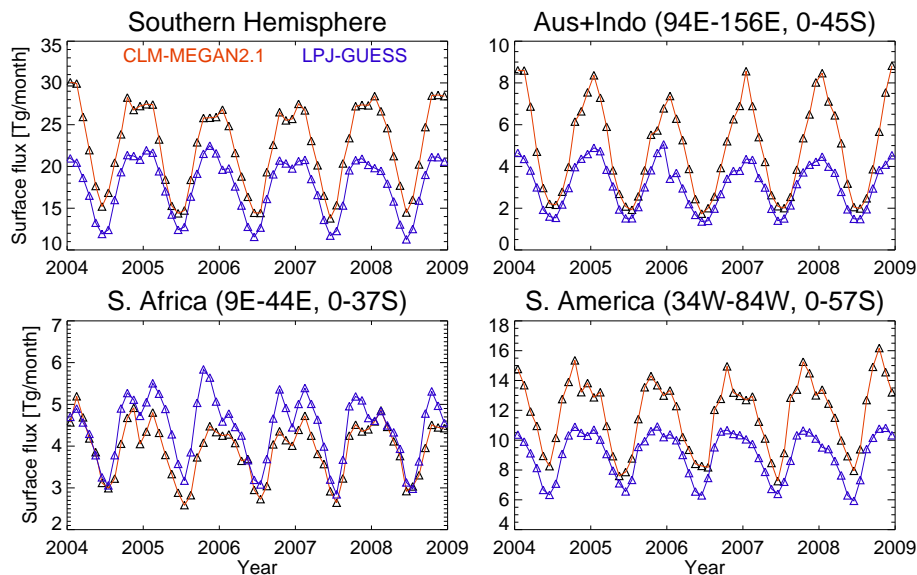
Figure 1. Regional emission fluxes for isoprene between 2004 and 2008 from the CLM-MEGANv2 and LPJ-GUESS emission inventories.

Full Screen / Esc

Printer-friendly Version

Interactive Discussion

Full Screen / Esc

Printer-friendly Version

Interactive Discussion
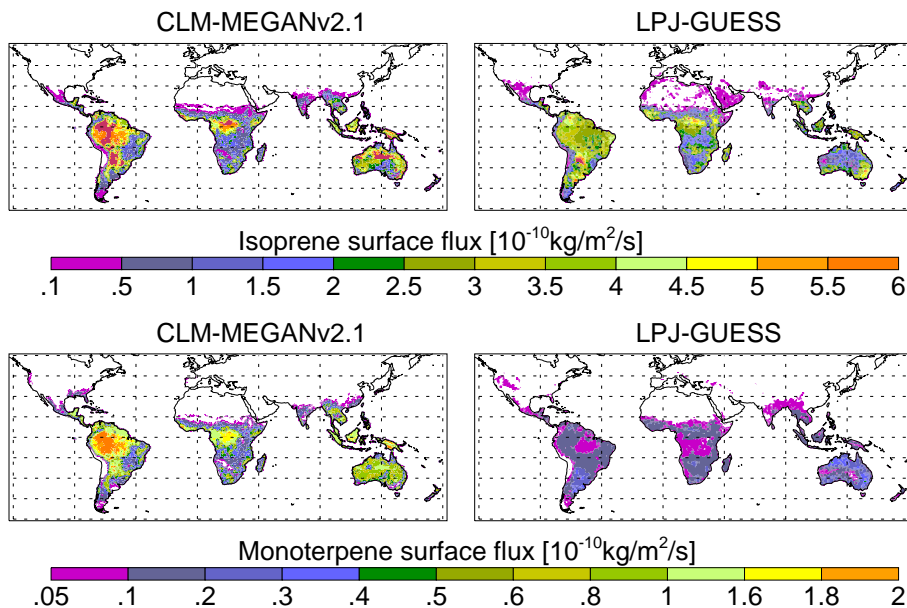
Figure 2. Isoprene and monoterpene emission distributions from CLM-MEGANv2.1 and LPJ-GUESS for January 2005.
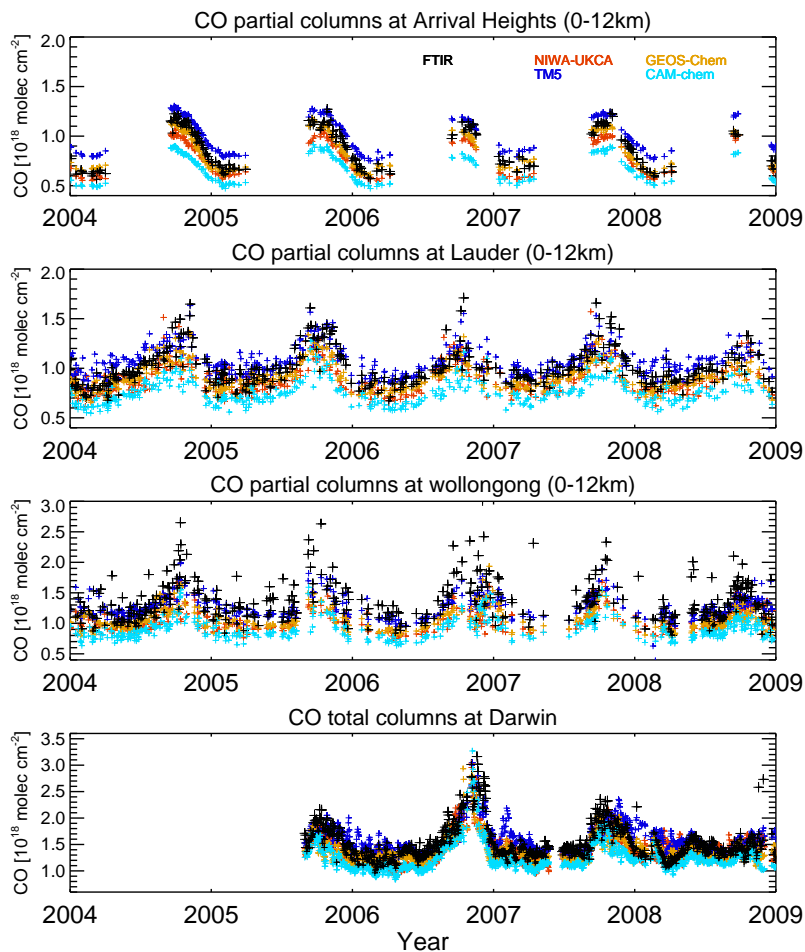
Figure 3. Modelled and observed daily mean FTIR CO columns at SH stations from 4 models. Simulations use CLM-MEGANv2.1 biogenic emissions.

Full Screen / Esc

Printer-friendly Version

Interactive Discussion
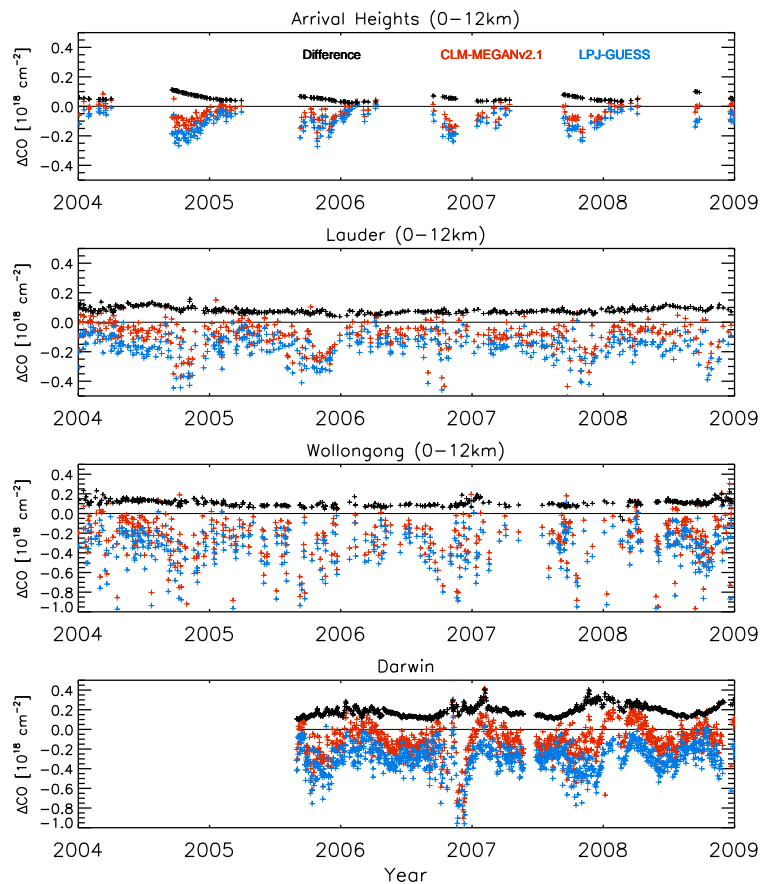
Figure 4. Deviations of model ensemble- and daily-mean CO columns from the observed FTIR CO columns with CLM-MEGANv2.1 simulation (red) and with LPJ-GUESS simulation (blue) respectively. The difference between the modelled CO columns from these two simulations are displayed in black symbols ($CO_{CLM-MEGANv2.1} - CO_{LPJ-GUESS}$).
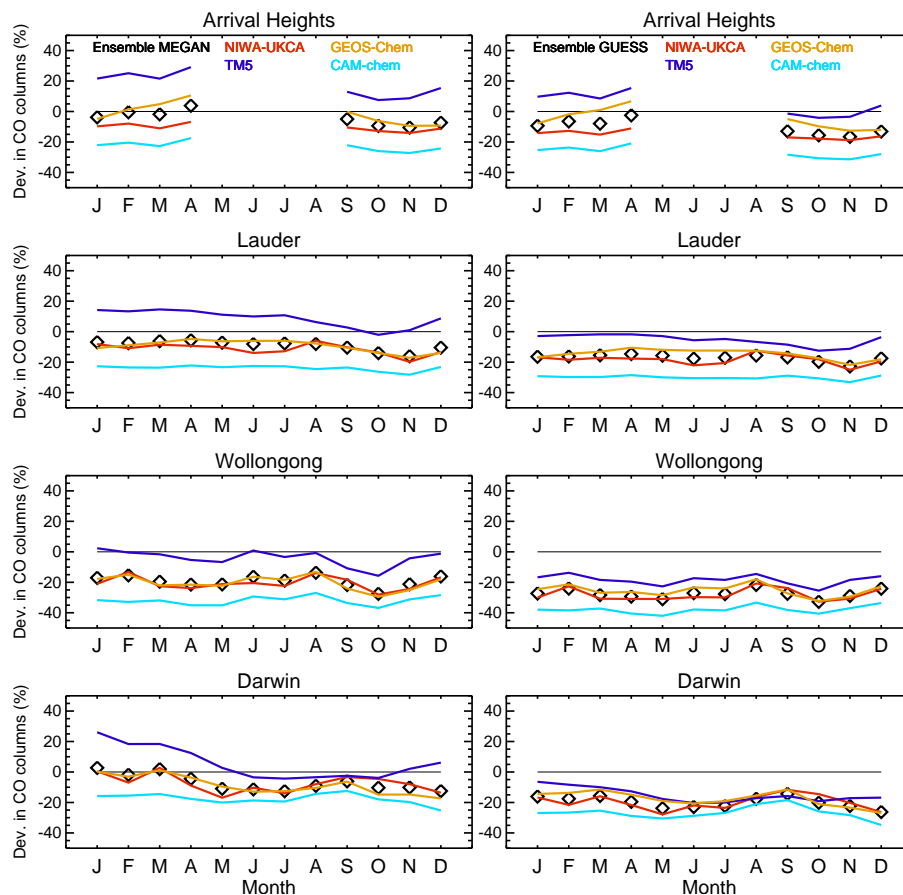
Figure 5. Percentage differences between modelled and observed multi-annual mean CO columns at Arrival Heights, Lauder, Wollongong, and Darwin from two simulations with CLM-MEGANv2.1 (left) and LPJ-GUESS emissions (right) respectively. Ensemble means are indicated by black symbols and individual models are by coloured lines.
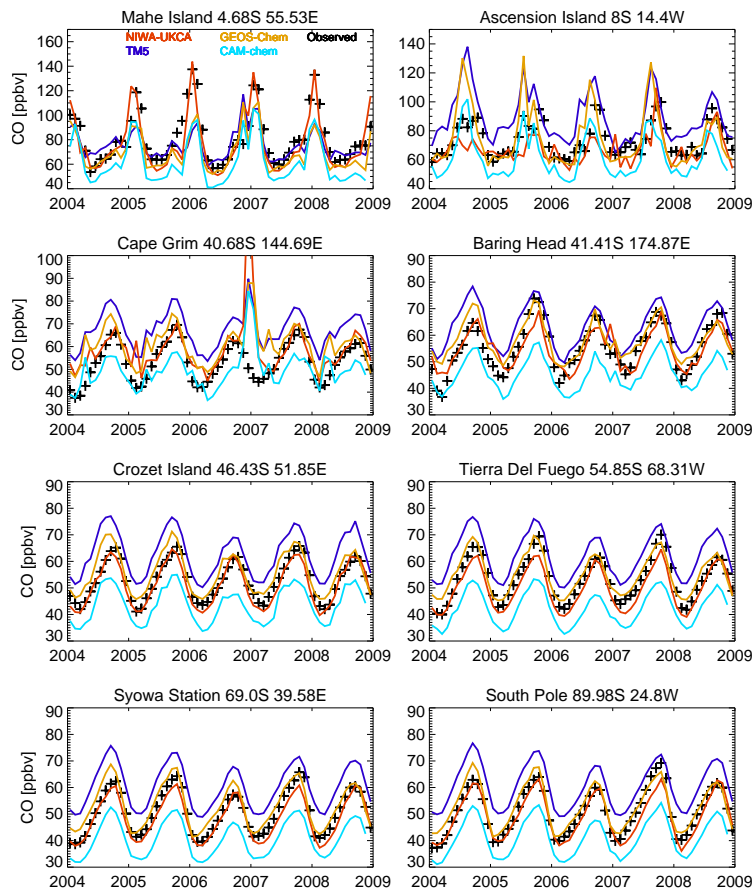
Figure 6. Modelled monthly mean surface CO with CLM-MEGANv2.1 emissions (coloured lines) and observed monthly mean surface CO at SH sites. Observations are from the NOAA GMD network (Novelli et al., 1998): http://www.esrl.noaa.gov/gmd/.

Full Screen / Esc

Printer-friendly Version

Interactive Discussion
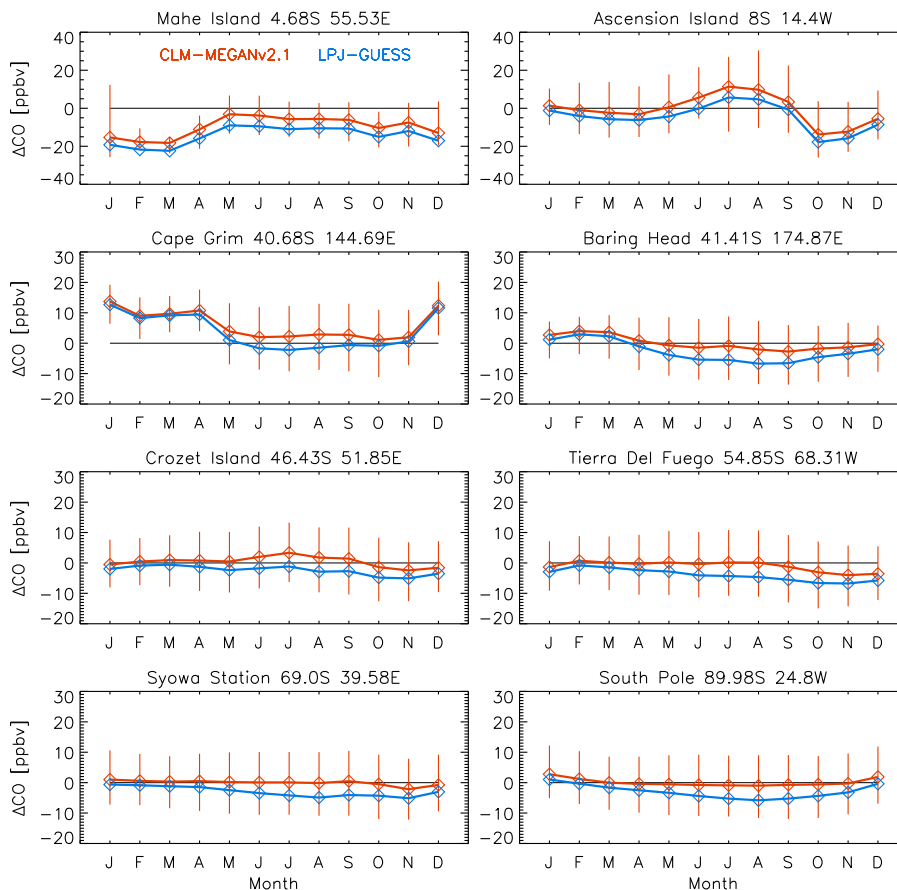
Figure 7. Deviations of ensemble and monthly mean surface CO from observed surface CO; red for CLM-MEGANv2.1 and blue for LPJ-GUESS simulations respectively. Model ranges are indicated by vertical bars from the CLM-MEGANv2.1 simulation.

Title Page

Abstract | Introduction

Conclusions | References

Tables | Figures

|◄ | ►|

◄ | ►

Back | Close

Full Screen / Esc

Printer-friendly Version

Interactive Discussion
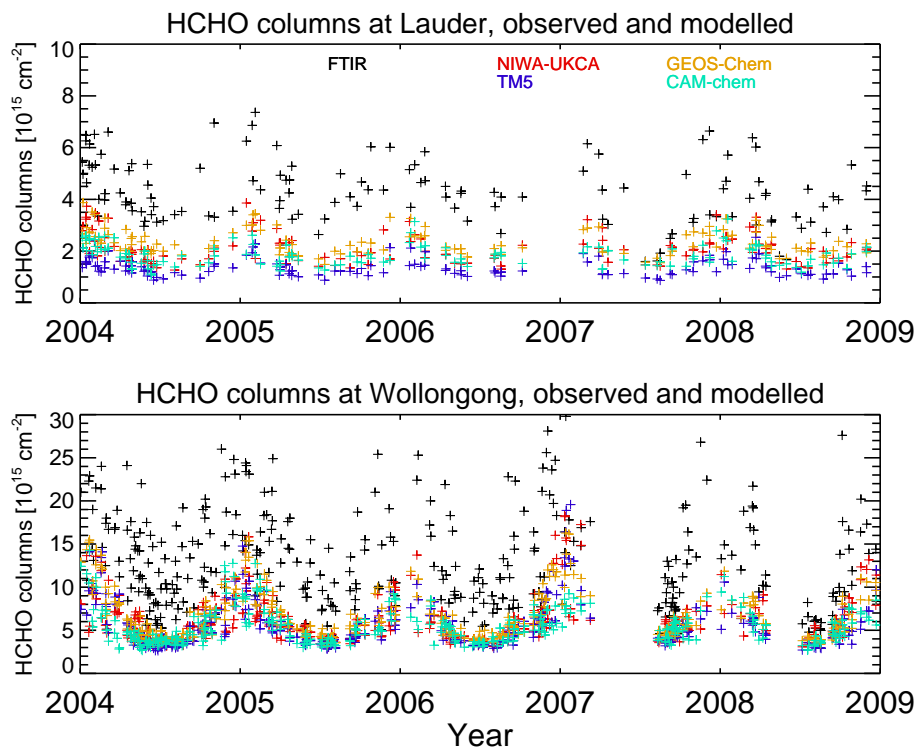
Figure 8. Modelled and observed daily mean FTIR HCHO columns at Lauder and Wollongong.
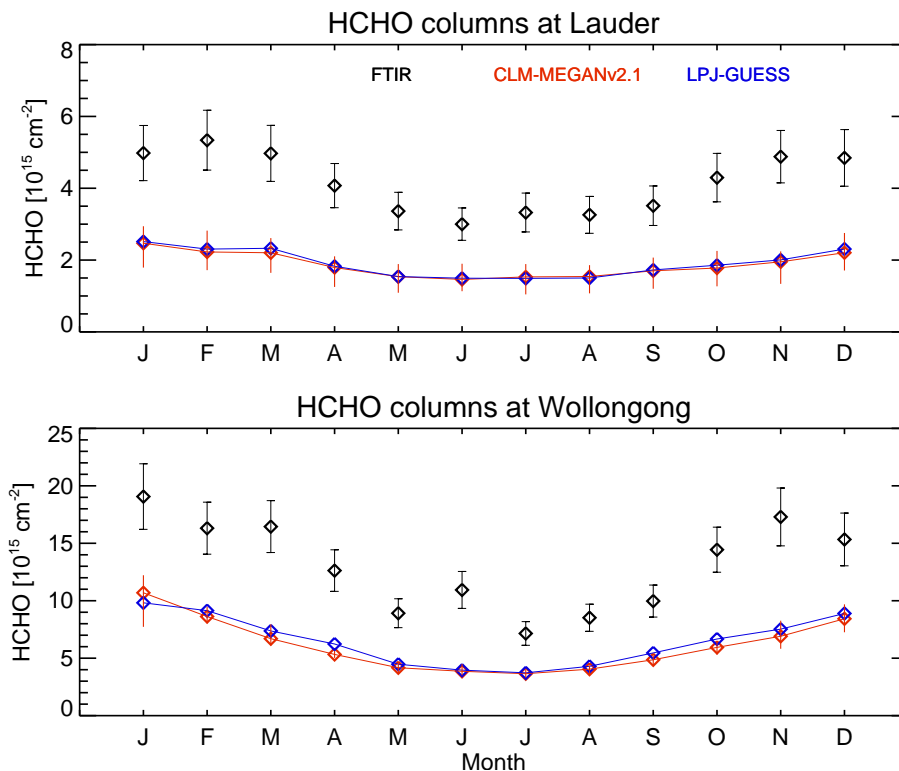
Figure 9. Observed (black symbols) FTIR multi-annual mean HCHO columns and ensemble and model mean from CLM-MEGANv2.1 (red) and LPJ-GUESS (blue) simulations. Measurement errors are shown by vertical bars (black). Model ranges from the CLM-MEGANv2.1 simulations are also given (coloured vertical bars).

Title Page

Abstract | Introduction

Conclusions | References

Tables | Figures

|◄ | ►|

◄ | ►

Back | Close

Full Screen / Esc

Printer-friendly Version

Interactive Discussion
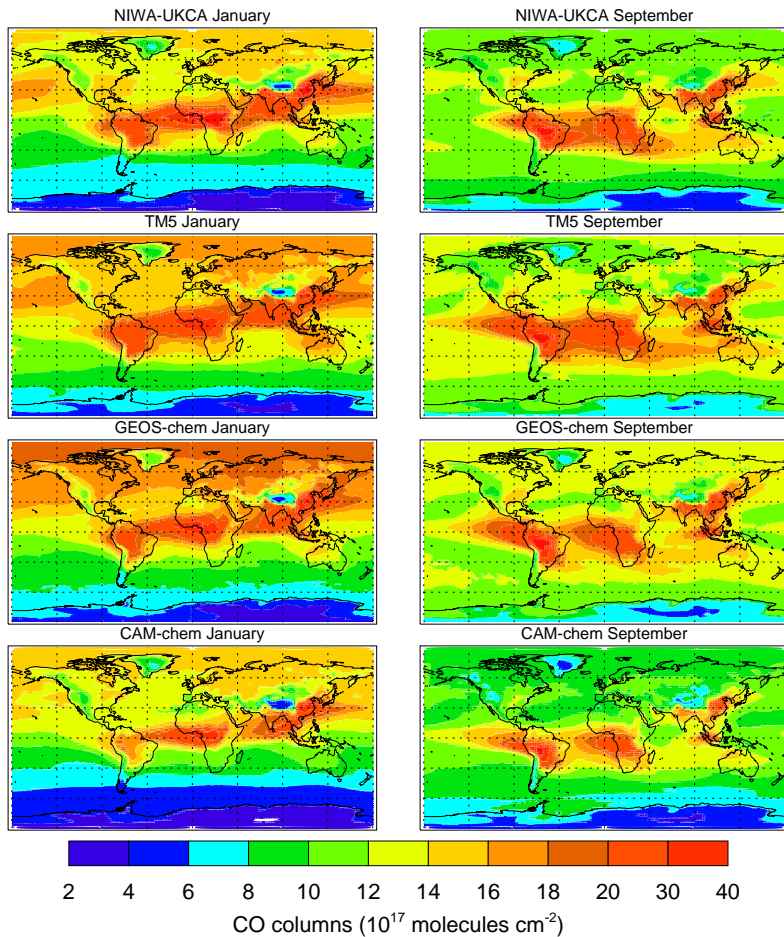
Figure 10. Tropospheric CO columns from 4 models for January (left) and September (right). Values are multi-annual means over 2004–2008.
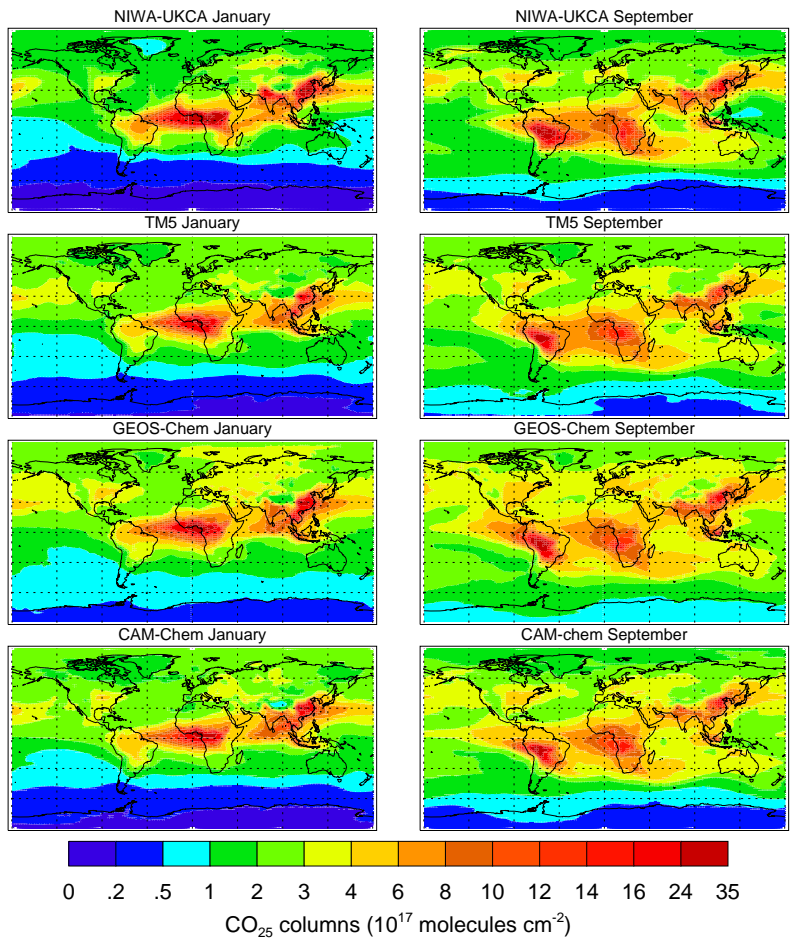
Figure 11. Tropospheric CO_{25} tracer columns from 4 models for January (left) and September (right) 2005.
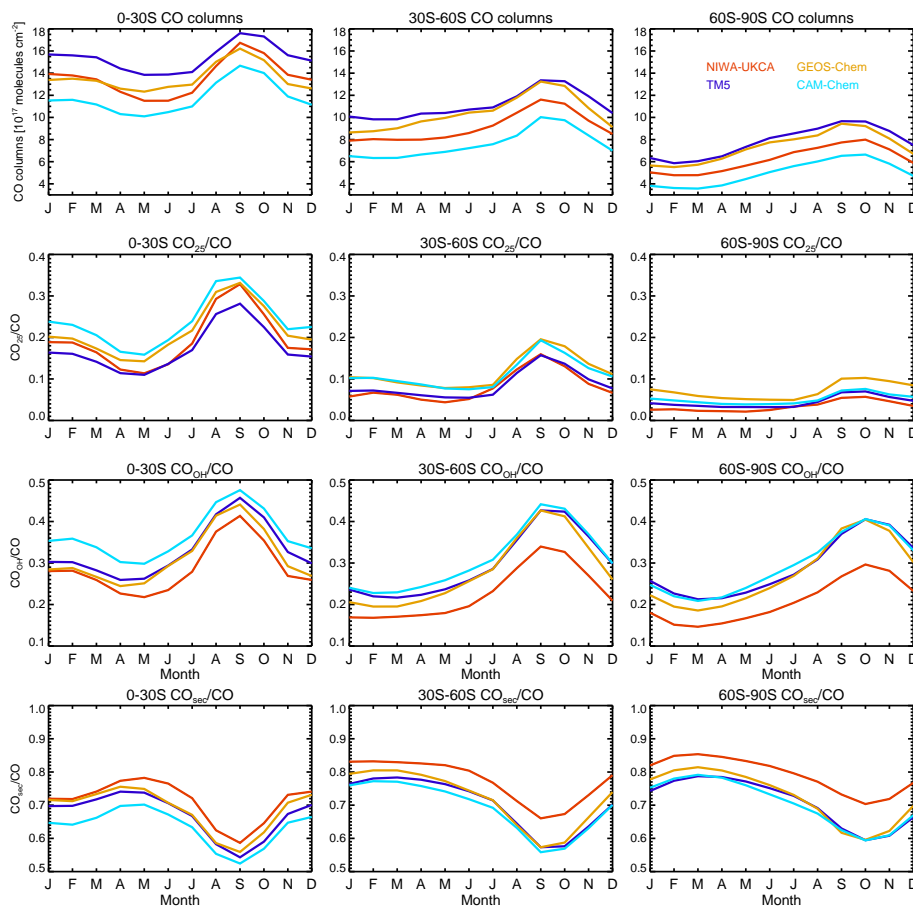
Figure 12. Monthly mean CO columns (top) and the ratio of CO_{25} to CO, CO_{OH} to CO, and CO_{sec} to CO columns averaged over three SH regions. Data are for the year 2005.

Discussion Paper | Discussion Paper | Discussion Paper | Discussion Paper

Title Page

Abstract | Introduction

Conclusions | References

Tables | Figures

|◄ | ►|

◄ | ►

Back | Close

Full Screen / Esc

Printer-friendly Version

Interactive Discussion
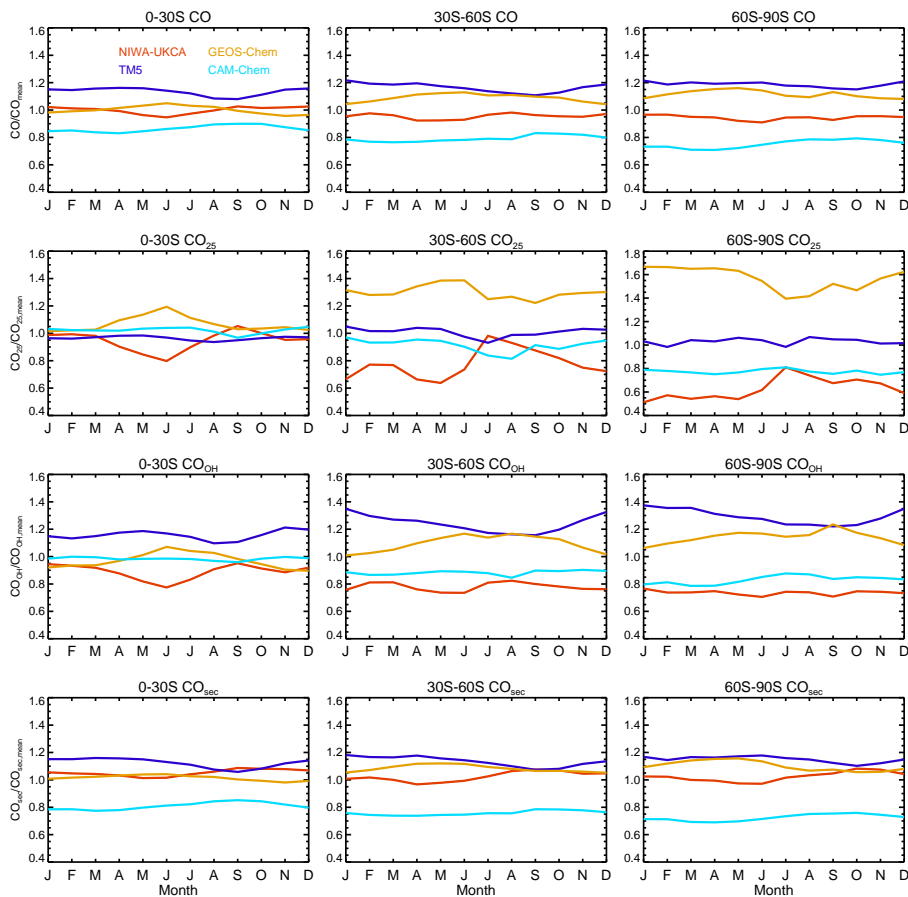
Figure 13. The ratio of individual models to the ensemble mean columns averaged over three SH regions (0–30° S, 30–60° S, and 60–90° S) for CO, CO_{25}, CO_{OH}, and CO_{sec}. Data are for the year 2005.

Title Page

Abstract | Introduction

Conclusions | References

Tables | Figures

◄ | ►

◄ | ►

Back | Close

Full Screen / Esc

Printer-friendly Version

Interactive Discussion
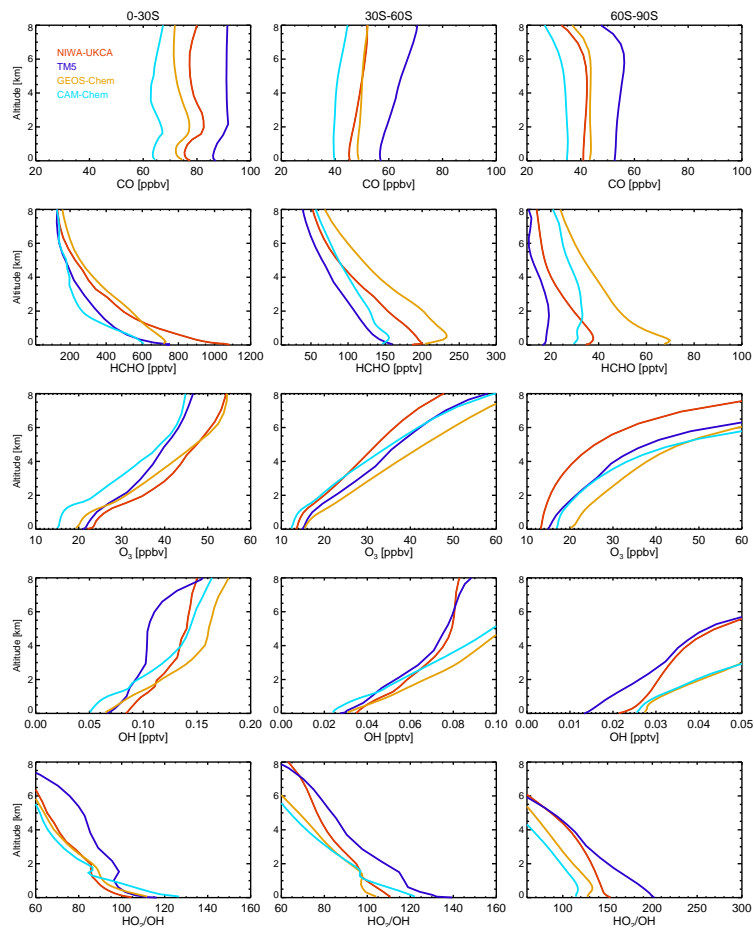
Figure 14. Monthly mean mixing ratios averaged over three SH regions (0–30° S, 30–60° S, and 60–90° S) for CO, HCHO, O_3, OH and the ratio of HO_2/OH. Data are for January 2005.

Title Page

Abstract | Introduction

Conclusions | References

Tables | Figures

|◄ | ►|

◄ | ►

Back | Close

Full Screen / Esc

Printer-friendly Version

Interactive Discussion
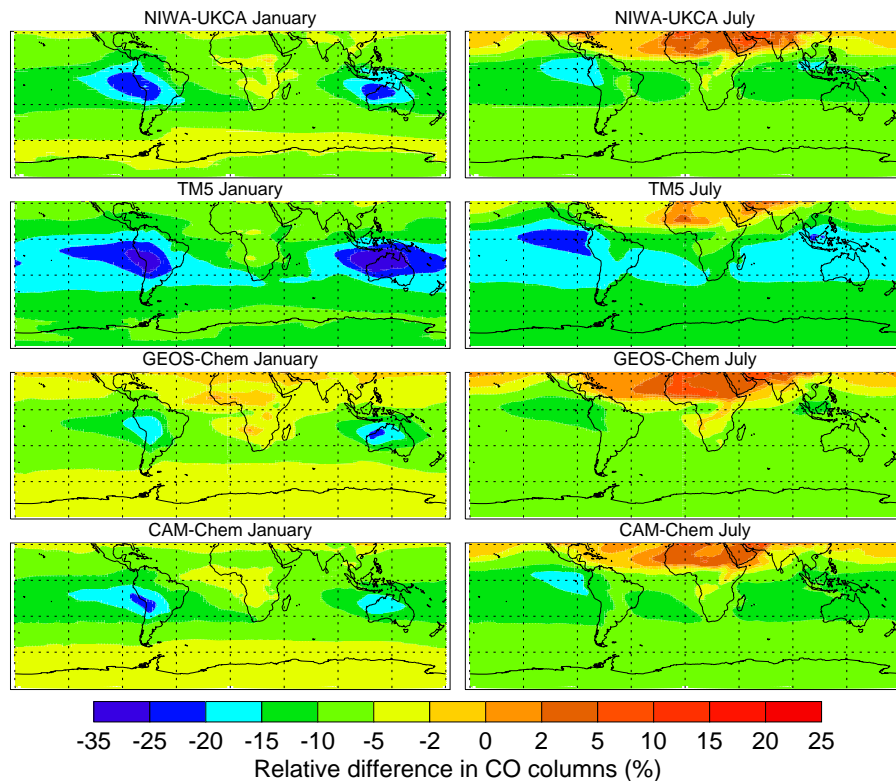
Figure 15. Relative differences (%) in multi-annual and ensemble mean modelled CO columns between the LPJ-GUESS and the CLM-MEGANv2.1 simulations from 4 models for January (left) and July (right). Results are expressed as "$100 \times (CO_{LPJ\text{-}GUESS} - CO_{CLM\text{-}MEGANv2.1})/CO_{CLM\text{-}MEGANv2.1}$".
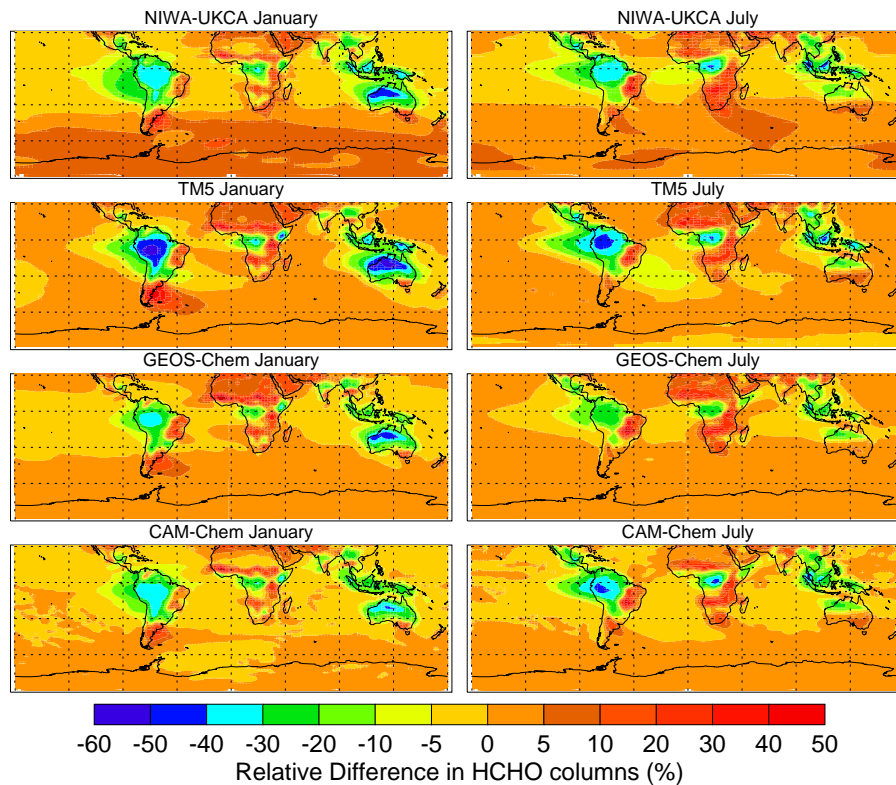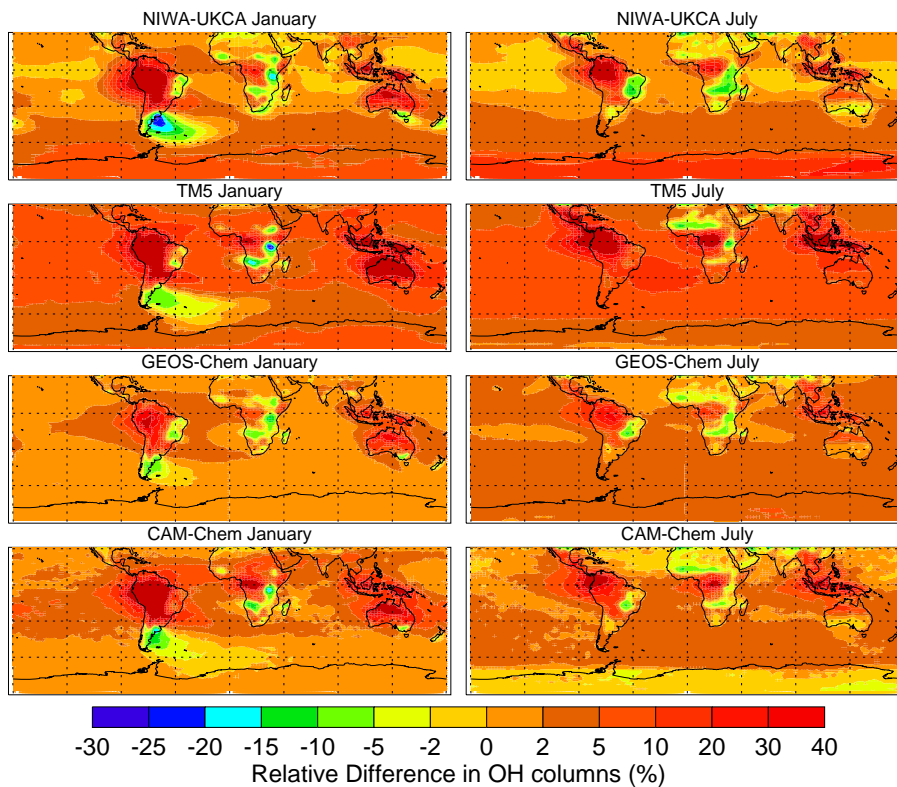
Figure 16. Same as Fig. 15, but for HCHO.

Title Page

Abstract | Introduction

Conclusions | References

Tables | Figures

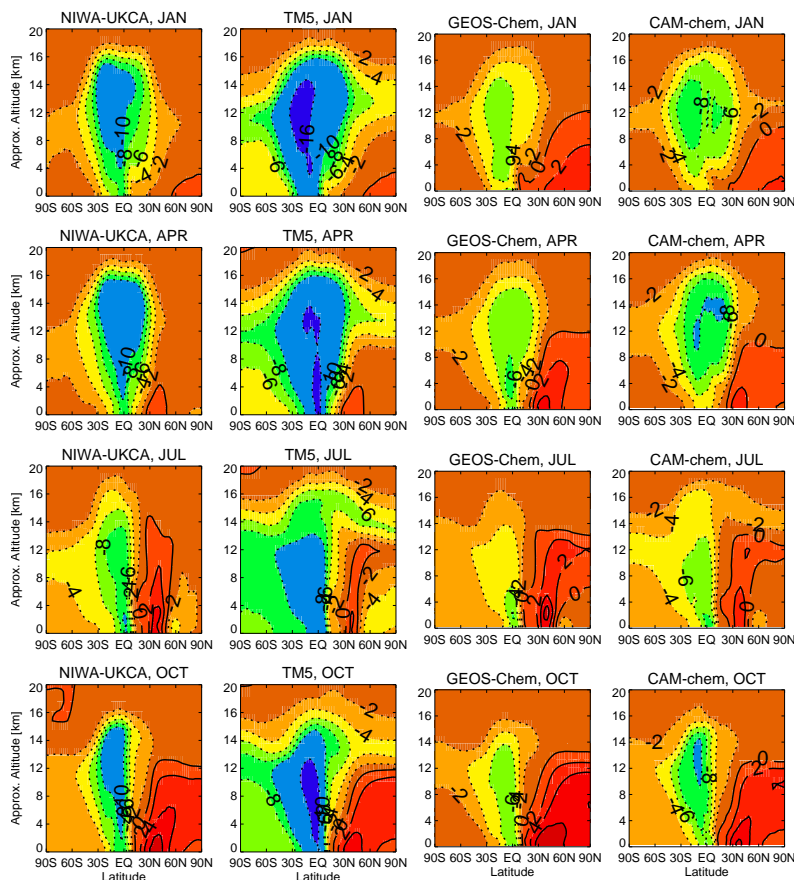|◄ | ►|

◄ | ►

Back | Close

Full Screen / Esc

Printer-friendly Version

Interactive Discussion

Figure 17. Same as Fig. 15, but for OH.

Figure 18. Zonal mean and monthly mean differences in CO [ppbv] between the LPJ-GUESS and the CLM-MEGANv2.1 simulations (expressed as "CO$_{LPJ\text{-}GUESS}$ – CO$_{CLM\text{-}MEGANv2.1}$") for January, April, July, and October. Data are averaged over 2004–2008.

Title Page

Abstract | Introduction

Conclusions | References

Tables | Figures

◀ | ▶

◀ | ▶

Back | Close

Full Screen / Esc

Printer-friendly Version

Interactive Discussion